Cell Reports

Article

STING signaling promotes NK cell antitumor immunity and maintains a reservoir of TCF-1^{+} NK cells

Graphical abstract

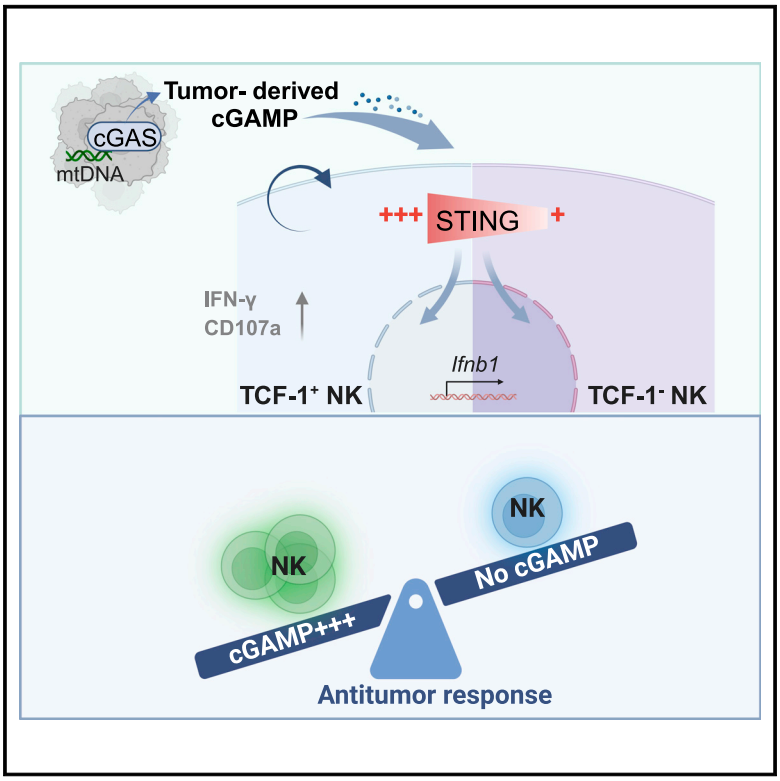

Authors

Lu Lu, Chao Yang, Xingyue Zhou, ..., Ao Zhang, Wen Di, Liufu Deng

Correspondence

dengliufu@sjtu.edu.cn

In brief

Lu et al. demonstrate that tumor-derived cGAMP transfer and subsequent cell-intrinsic STING engagement prime NK cell antitumor response. They identify a previously unrecognized role of STING signaling in maintaining a reservoir of TCF-1^{+} NK cells in tumors. STING agonism represents a promising therapeutic strategy to enhance NK cell-based cancer immunotherapy.

Highlights

- Intrinsic STING in NK cells promotes their antitumor activity
- Tumor cell-derived mtDNA and cGAS facilitates NK cell antitumor response
- STING signaling maintains a reservoir of TCF-1^{+} NK cells in tumors
- STING agonism strengthens TCF-1^{+} NK cells function in humans

Lu et al., 2023, Cell Reports *42*, 113108
September 26, 2023
https://doi.org/10.1016/j.celrep.2023.113108

CellPress

Cell Reports

CellPress
OPEN ACCESS

Article

STING signaling promotes NK cell antitumor immunity and maintains a reservoir of TCF-1^{+} NK cells

Lu Lu,[1,4] Chao Yang,[1,4] Xingyue Zhou,[1] Lingling Wu,[1,2] Xiaochuan Hong,[1,2] Wenwen Li,[2] Xinran Wang,[3] Yuanqin Yang,[2] Dongqing Cao,[2] Ao Zhang,[1] Wen Di,[3] and Liufu Deng[1,5,*]

[1]Shanghai Frontiers Science Center of Drug Target Identification and Delivery, National Key Laboratory of Innovative Immunotherapy, School of Pharmacy, Shanghai Jiao Tong University, Shanghai 200240, China

[2]Shanghai Institute of Immunology, Department of Immunology and Microbiology, Shanghai Jiao Tong University School of Medicine, Shanghai 200025, China

[3]Department of Obstetrics and Gynecology, Shanghai Key Laboratory of Gynecologic Oncology, Ren Ji Hospital, Shanghai Jiao Tong University School of Medicine, Shanghai 200127, China

[4]These authors contributed equally

[5]Lead contact

*Correspondence: dengliufu@sjtu.edu.cn

https://doi.org/10.1016/j.celrep.2023.113108

SUMMARY

Natural killer (NK) cells are cytotoxic innate lymphocytes that eradicate tumor cells. Inducing durable antitumor immune responses by NK cells represents a major priority of cancer immunotherapy. While cytosolic DNA sensing plays an essential role in initiating antitumor immunity, the role of NK cell-intrinsic STING signaling remains unclear. Here, we find that NK cell-intrinsic STING promotes antitumor responses and maintains a reservoir of TCF-1^{+} NK cells. In contrast, tumor cell-intrinsic cGAS and mtDNA are required for NK cell antitumor activity, indicating that tumor mtDNA recognition by cGAS partially triggers NK cell-intrinsic STING activation. Moreover, addition of cGAMP enables STING activation and type I interferon production in NK cells, thereby supporting the activation of NK cells *in vitro*. In humans, STING agonism promotes the expansion of TCF-1^{+} NK cells. This study provides insight into understanding how STING signaling drives NK cell antitumor immunity and the development of NK cell-based cancer immunotherapy.

INTRODUCTION

Innate immune sensing has been identified as a key initiator for innate and adaptive antitumor immune responses in both natural and therapeutic biological contexts, such as radiotherapy, PARP inhibition, and immunotherapy.[1–7] Among the multiple nucleic acid-sensing pathways, the cyclic GMP-AMP synthase (cGAS)-STING cascade can play a central role in breaking tumor immune tolerance by accelerating the cancer-immunity cycle.[5,8,9] Considering the therapeutic potential of STING agonism, STING function has been characterized in tumor cells and various immune cell subsets.[5,9] Upon intrinsic or extrinsic stress, the cGAS-STING pathway is activated by cytoplasmic enrichment with genomic or mitochondrial DNA (gDNA or mtDNA) to promote immunogenicity of tumor cells and activity of dendritic cells.[1,3,10–12] However, in CD8^{+} T cells, the cGAS-STING cascade acts as an intrinsic modulator for the formation and maintenance of stem cell-like properties,[13] suggesting that STING signaling may be essential for the activity of cytotoxic lymphocytes, including CD8^{+} T cells and natural killer (NK) cells. It is therefore conceivable that a comprehensive understanding of STING function in cytotoxic lymphocytes could guide the development of therapeutic strategies for CD8^{+} T cell-resistant tumors.

NK cells are cytotoxic lymphocytes that have the ability to kill tumor cells and secrete inflammatory cytokines.[14] Due to this role in tumor inhibition, NK cells therefore provide key functions in tumor immune surveillance, particularly in preventing tumor metastasis.[15] Sufficient stimulation of tumor-infiltrating NK cell function remains a central challenge in the development of cancer immunotherapy.[16–19] NK cells can be primed via several different modes, including the engagement of the stimulatory receptors, combined exposure to IL-12, IL-15, and IL-18 cytokines, and stimulation of RNA sensing.[18,20] Interestingly, memory-like NK cells have been defined as T and B cell counterparts that have differentiated to acquire immunological memory.[21–23] NK cells with a memory-like phenotype exhibit characteristically high expression of the transcription factor TCF-1.[24,25] Stimulation of immature NK cells with a cytokine cocktail containing IL-12, IL-18, and IL-15 leads to differentiation into memory-like NK cells,[26,27] which can provide an enhanced antitumor response in chimeric antigen receptor (CAR)-NK therapies.[28] In humans, NK cells are divided into two major subsets: CD56^{dim}CD16^{+} cytotoxic NK cells and

$CD56^{hi}CD16^{-}$ cytokine-secreting NK cells.[29] Pre-activation of the $CD56^{hi}$ NK cells in PBMCs with IL-15 augments their antitumor responses.[30] Therefore, understanding the molecular mechanism that sustains persistent NK cell responses will provide strong rationales for the design of NK cell-based cancer immunotherapy.

Extrinsic STING pathway activation of NK cells has been previously described in tumor models.[5,7,31] Tumor-derived cGAMP triggers host STING activation and subsequent type I IFN production, which enhances antitumor activity by NK cells.[31] Consistent with these effects, treatment with STING agonists can induce NK cell activation to attack $CD8^{+}$ T cell-resistant tumors.[7] However, the specific contributions of cell-intrinsic STING signaling in NK cell activity have not been determined. As a secondary messenger, cGAMP can be transported between different cell types, including tumor cells and immune cells, thereby forming a new modality for intercellular interactions.[9] Furthermore, it is likely that the recipient cells of cGAMP transfer are not restricted to the aforementioned cell types. Current strategies for NK cell activation rely on the use of ligands and cytokines,[17] but it is also unknown whether exogenous cGAMP can serve as a stimulator for NK cell activation in a cell-intrinsic fashion. Type I interferon (IFN) signaling has been demonstrated to enhance the activation of NK cells in malignancies with STING agonist administration as well as in acute infections.[7,32,33] Moreover, the direct action on NK cells by type I IFNs is observed in the tumor therapeutics and infection settings.[7,34] Thus, it is likely that the amount and origin of type I IFN production dictates the pattern of cell circuits for NK cell antitumor activity.

In this study, we show that intrinsic STING signaling facilitates NK cell antitumor immunity and the expansion of $TCF\text{-}1^{+}$ NK cells. Moreover, mtDNA sensing by cGAS in tumor cells promotes STING-dependent NK cell activity; also, exogenous cGAMP treatment facilitates NK cell activation *in vitro* through autocrine STING-mediated type I IFN signaling. In addition, prolonged incubation with cGAMP expands the formation of human $TCF\text{-}1^{+}CD56^{+}$ NK cells. Therefore, our findings provide a mechanistic foundation for understanding NK cell antitumor activity, and suggest alternative strategies for enhancing NK cell-based cancer therapies.

RESULTS

NK cell-specific STING potentiates their antitumor activity

NK cells play an essential role in detecting and killing tumor cells, and the STING pathway particularly contributes to its antitumor activity in a cell-extrinsic manner.[5,17,31] To better understand the patterns of STING expression in human NK cells, we conducted intracellular staining for STING in the $CD3^{-}CD56^{+}$ NK cells in peripheral blood samples of patients with cancer and healthy volunteers using a flow cytometry gating strategy (Figures S1A and S1B). STING expression was diminished in the NK cell population in patients with cancer compared with its expression in healthy volunteers (Figure 1A). We then characterized its expression profile in tumor-infiltrating NK cells from primary tumors and metastatic nodules of patients with gynecological cancer using the same method. We found that STING expression was decreased in metastatic tumors compared with that in matched primary tumors (Figure 1B). Furthermore, a lower STING expression was observed in NK cells from primary tumors versus PBMCs in the same patients (Figure S1C). These findings indicate that STING expression is attenuated in tumor-infiltrating NK cells of patients with cancer, which suggests the possibility that cell-intrinsic STING expression may be correlated with the ability of NK cells to control tumor.

To assess whether STING functions as a determining factor in NK cell-mediated antitumor activity, we crossed $STING^{f/f}$ mice with $Ncr1^{iCre}$ mice to obtain $Ncr1^{iCre}STING^{f/f}$ mice, in which STING was conditionally depleted in NK cells. The deletion of STING in NK cells from spleens of $Ncr1^{iCre}STING^{f/f}$ mice was verified by western blot (Figure S1D). Consistent with a previous study, we confirmed that NK cells rather than $CD8^{+}$ T cells played a central role in inhibiting B16F10 tumor metastasis (Figure S1E). To examine whether STING deficiency negatively affected the antitumor response of NK cells, we intravenously injected B16F10 cells into $Ncr1^{iCre}STING^{f/f}$ mice, with $STING^{f/f}$ mice serving as controls. We observed that the number of melanoma nodules was increased in the lung tissue of $Ncr1^{iCre}STING^{f/f}$ mice compared with that in $STING^{f/f}$ littermates (Figure 1C), suggesting that NK cell-intrinsic STING contributes to the limitation of tumor metastasis.

Although STING acts importantly in myeloid cells within tumors, we further demonstrated that STING action in NK cells contributes to robust antitumor responses as well. To test whether this effect could also be observed in a subcutaneous tumor model, we knocked out B2M in both B16F10 and MC38 tumor cell lines, which abolished surface expression of MHC class I molecules and heightened sensitivity for NK cell recognition (Figure S1F). Consistent with our initial results, targeted knockout of STING in NK cells resulted in accelerated tumor growth in both B16F10-$B2M^{-/-}$ and MC38-$B2M^{-/-}$ models (Figures 1D and 1E). To rule out the possibility that Cre may raise unexpected effects perhaps due to off-target DNA nicking in our setting, we injected B16F10 (intravenously) and MC38-$B2M^{-/-}$ (subcutaneously) into $Ncr1^{iCre}STING^{f/f}$ mice, respectively, with $Ncr1^{iCre}$ mice serving as controls. Consistent with our initial results, the accelerated tumor growth was observed in $Ncr1^{iCre}STING^{f/f}$ mice compared with $Ncr1^{iCre}$ mice (Figures S1G and S1H). Taken together, these results indicate that NK cell-intrinsic STING is essential for tumor immunosurveillance.

NK cell-intrinsic STING promotes antitumor immune responses

We next sought to examine whether STING contributes to the responsiveness of tumor-infiltrating NK cells. We found that STING deficiency resulted in lower antitumor activity of NK cells characterized by IFN-γ and CD107a production in metastatic B16F10 tumors (Figures 2A and 2B). In agreement with the above observations in metastatic tumors, the expression of IFN-γ and CD107a was impaired in STING-deficient NK cells compared with wild-type (WT) NK cells from subcutaneous MC38-$B2M^{-/-}$ tumors (Figures 2C and 2D). Collectively, these data suggest that inherent STING signaling is required for NK

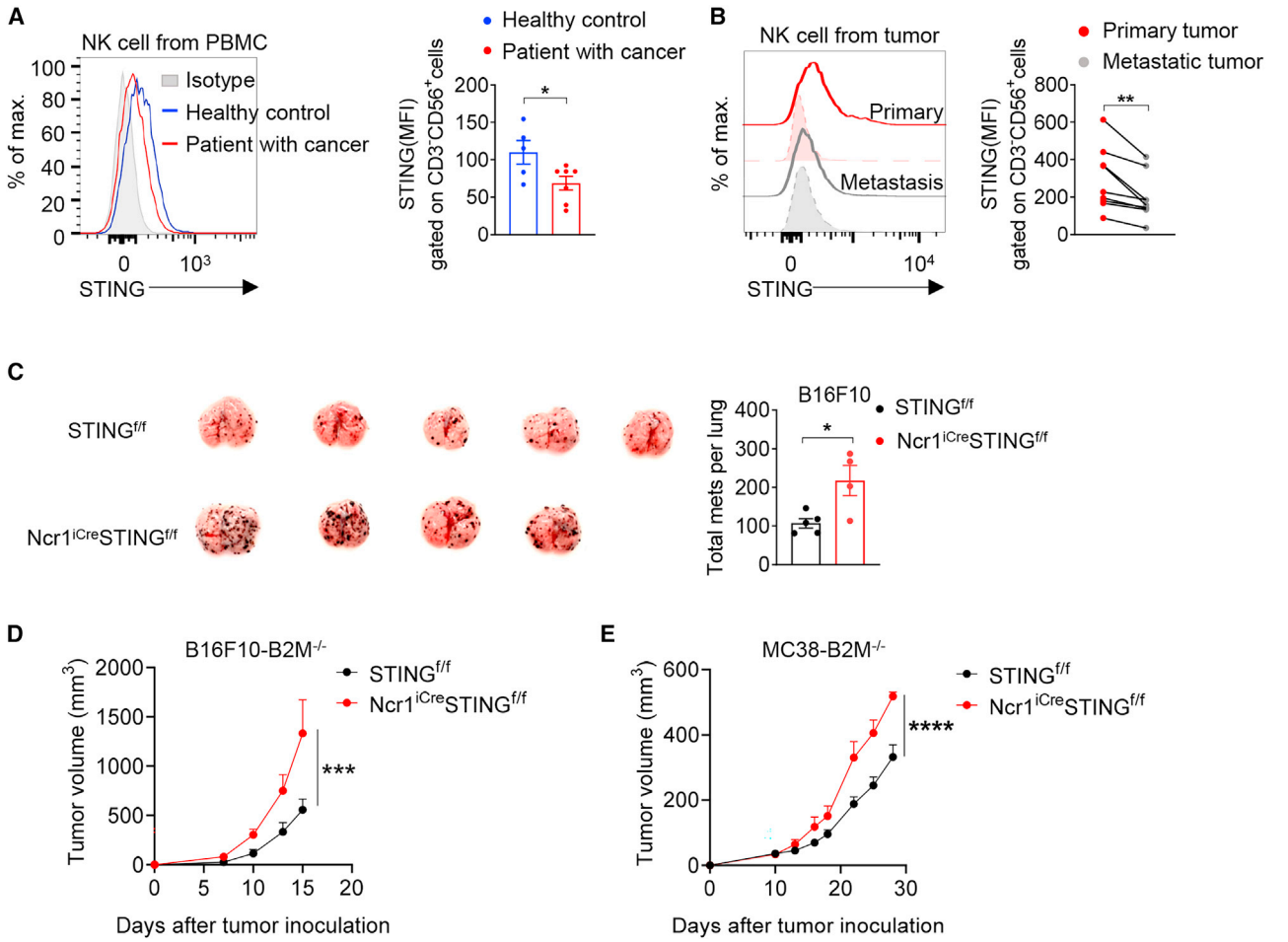

Figure 1. Intrinsic STING in NK cells mediates their antitumor responses

(A) Representative histogram (left) and mean fluorescent intensity (MFI) summary (right) showing STING expression in NK cells from peripheral blood of healthy volunteers (n = 5) and patients (n = 7, Table S2, patients 1–7).

(B) Representative histogram (left) and MFI summary (right) showing STING expression in NK cells from patients with primary tumor and metastatic tumor (carcinosarcoma [n = 1], ovarian cancer [n = 8], Table S2, patients 8–16). Each dot represents one donor in (A and B).

(C) Representative appearance of lung metastatic tumors (left) and the number of metastatic tumor nodules (right). STING$^{f/f}$ and Ncr1^{iCre}STING$^{f/f}$ mice (n = 4–5) were intravenously injected with 2 × 10^5 B16F10 cells. Mice were sacrificed on day 14 after tumor injection.

(D and E) Tumor growth in STING$^{f/f}$ and Ncr1^{iCre}STING$^{f/f}$ mice; 5 × 10^5 B16F10-B2M$^{-/-}$ (D) and MC38-B2M$^{-/-}$ (E) tumor cells were subcutaneously injected into STING$^{f/f}$ and Ncr1^{iCre}STING$^{f/f}$ mice (n = 3–6), respectively. Representative data are shown from two or three independent experiments. Data are represented as mean ± SEM. *p < 0.05, **p < 0.01, ***p < 0.001, ****p < 0.0001 by unpaired Student's t test in (A and C), paired Student's t test in (B), two-way ANOVA in (D and E). See also Figure S1 and Table S2.

cell responsiveness that leads to IFN-γ and CD107a production after stimulation.

To rule out the possibility that lack of STING may induce developmental defects in the NK cell differentiation program, we also analyzed the proportion and activation of NK cells in the lungs and spleens of naive Ncr1^{iCre}STING$^{f/f}$ and STING$^{f/f}$ mice. The results showed that the percentages of total NK cells and CD69$^+$ NK cells were equivalent between Ncr1^{iCre}STING$^{f/f}$ and STING$^{f/f}$ mice (Figures S2A and S2B). In addition, the activating receptor NKp46 expression was unaffected in Ncr1^{iCre}STING$^{f/f}$ mice compared with STING$^{f/f}$ mice (Figure S2C). These results indicate that the development and NKp46 expression of NK cells are comparable between Ncr1^{iCre}STING$^{f/f}$ and STING$^{f/f}$ mice.

Tumor cell mtDNA recognition by cGAS facilitates NK cell antitumor activity

Previous studies have demonstrated that cGAS functions as a central cytoplasmic DNA sensor to prime the STING signal cascade as part of the antitumor immune response.[9] To examine whether cGAS is also required for antitumor activity of NK cells, we crossed cGAS$^{f/f}$ mice with Ncr1^{iCre} mice to obtain Ncr1^{iCre}cGAS$^{f/f}$ mice in which cGAS was conditionally knocked out in NK cells. However, conditional depletion of cGAS in NK cells did not affect the number of metastatic tumor nodules, indicating that cGAS in NK cells does not contribute to the antitumor response (Figure 3A). We then used mice harboring whole-body knockout of cGAS to

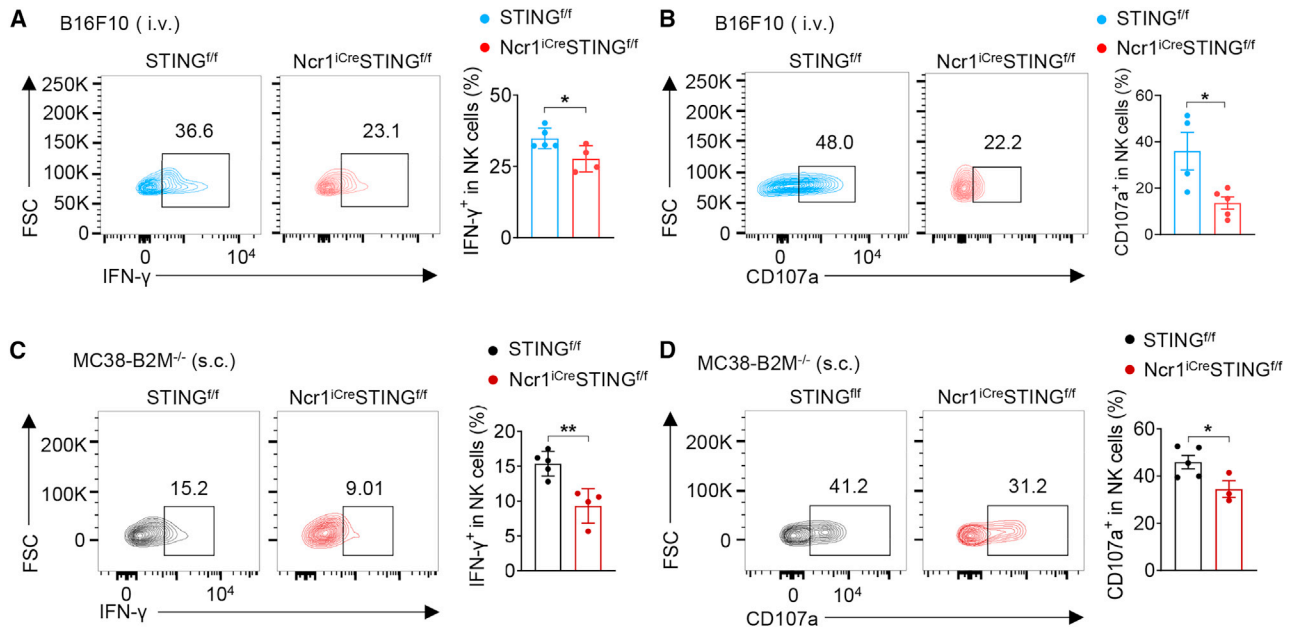

Figure 2. STING promotes NK cell functionality in tumors

(A and B) B16F10 cells (2–3 × 10^5) were intravenously injected into STING$^{f/f}$ and Ncr1^{iCre}STING$^{f/f}$ mice, respectively (n = 4–5). Lungs were harvested and stained for flow cytometry on day 14 after tumor injection after *ex vivo* stimulation with cell stimulation cocktail (containing PMA, ionomycin, brefeldin A, and monensin). Representative flow plots and quantification of IFN-γ$^+$ (A) and CD107a$^+$ (B) cells in NK cells from the lungs of STING$^{f/f}$ and Ncr1^{iCre}STING$^{f/f}$ tumor-bearing mice. (C and D) MC38-B2M$^{-/-}$ cells (5 × 10^5) were subcutaneously injected into STING$^{f/f}$ and Ncr1^{iCre}STING$^{f/f}$ mice, respectively (n = 3–5). Tumors were harvested on day 14 after injection and stained for flow cytometry after *ex vivo* stimulation with cell stimulation cocktail. Representative flow plots and quantification of IFN-γ$^+$ (C) and CD107a$^+$ (D) cells in NK cells from the subcutaneous tumors. Representative data are shown from two or three independent experiments. Data are represented as mean ± SEM. *p < 0.05, **p < 0.01 by unpaired Student's t test in (A–D). See also Figure S2.

investigate whether cGAS is involved in host antitumor activity. Similarly, loss of cGAS in the host had no obvious effect on metastatic tumor nodule formation (Figure 3B). These results suggest that host cGAS does not participate in NK cell antitumor activity.

It has been demonstrated that intratumoral macrophages, NK, and T cells are able to sense extracellular cGAMP in murine tumors.[35] Considering the phenotypic differences between host NK cells harboring STING or cGAS knockout, we then focused our attention on cGAS in tumor cells to further explore whether tumor-derived cGAS contributes to antitumor response. To this end, we first established stable cGAS$^{-/-}$ and STING$^{-/-}$ tumor cell lines using CRISPR-Cas9 technology. We then intravenously injected those tumor cells into WT mice and monitored the metastatic tumor burden and survival of tumor-bearing mice. The loss of cGAS in B16 tumor cells resulted in a marked increase in metastatic tumor nodules (Figure 3C). Likewise, cGAS deficiency in tumor cells led to lower survival rates in both B16F10 and MC38 tumor-bearing mice (Figures S3A and S3B), which was consistent with the previous findings.[31] In contrast, STING ablation in tumor cells prolonged the survival of mice in both tumor models (Figures S3A and S3B), suggesting that tumor cell-intrinsic STING exerts a totally different role in tumor metastasis compared with tumor cell-intrinsic cGAS. Collectively, these results indicate that tumor cell-intrinsic cGAS and NK cell-intrinsic STING cooperatively sustain NK cell antitumor activity via cGAMP transfer.

We further investigated whether tumor cell-intrinsic cGAS acts as a trigger of NK cell antitumor immune response. Knockout of cGAS in tumor cells decreased IFN-γ production in tumor-infiltrating NK cells (Figure 3D). In agreement with these results, lack of cGAS in tumor cells reduced CD107a expression in tumor-infiltrating NK cells (Figure 3E). These results indicated that tumor cell-intrinsic cGAS is required for the antitumor activity of NK cells. To confirm our finding that tumor cell-intrinsic cGAS is responsible for activation of STING in NK cells, we further assessed the molecular pathway in tumor-infiltrating NK cells by assessing the phosphorylation of TBK1, a downstream target of the STING pathway. Our results demonstrated that cGAS deficiency in tumor cells actually dampened TBK1 phosphorylation in NK cells (Figure S3C). In addition, these different lines of evidence suggest that tumor cell-derived cGAMP is responsible for the activation of STING in NK cells via intercellular communication.

Since cGAS is activated by the enrichment of cytosolic DNA that originates from multiple sources, including genomic, mitochondrial, and exogenous origins,[9] we next sought to determine the source of cytosolic DNA. For this purpose, we isolated CD45$^-$ tdTomato$^+$ MC38 tumor cells from lung tissues at 3 days after intravenous injection of tdTomato-labeled MC38 tumor cells into WT mice. The purified cytosolic extracts were analyzed by real-time qPCR assays of *Tert* and *Dloop1*, genomic and mitochondrial DNA (mtDNA) markers, respectively. We observed that the cytosolic levels of these mtDNA fragments were increased in metastatic tumor cells compared with those

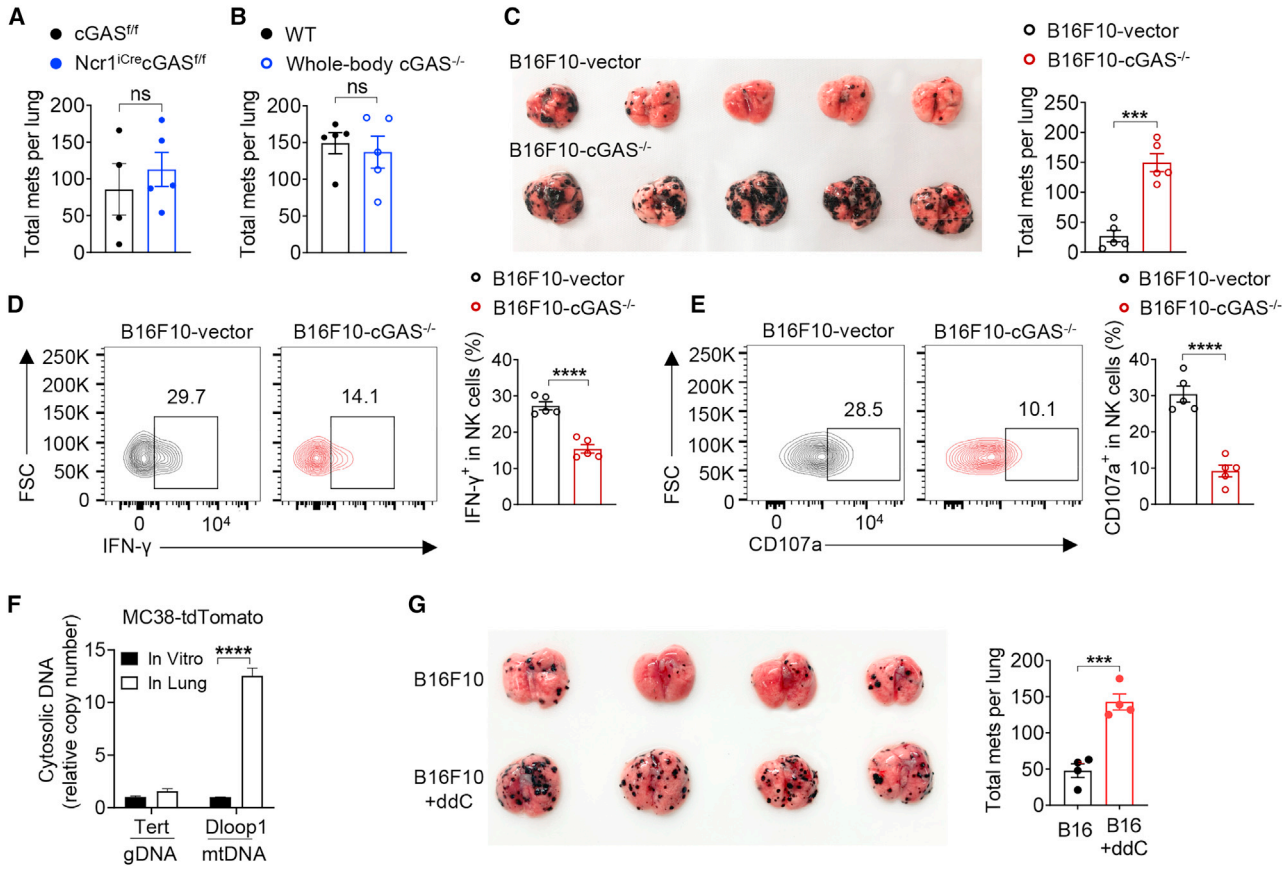

Figure 3. Tumor cell-derived mtDNA recognition by cGAS promotes NK cell antitumor activity

(A) cGAS$^{f/f}$ and Ncr1^{iCre}cGAS$^{f/f}$ mice (n = 4–5) were intravenously injected with 3 × 10^5 B16F10 cells. Quantification of metastatic tumor nodules after 14 days.

(B) WT and cGAS$^{-/-}$ mice (n = 5) were intravenously injected with 2 × 10^5 B16F10 cells. Quantification of metastatic tumor nodules after 14 days.

(C–E) B16F10-vector and B16F10-cGAS$^{-/-}$ cells (2 × 10^5) were intravenously injected into WT mice (n = 5). Quantification of metastatic tumor nodules and flow cytometry analysis on day 14 after injection. Representative appearance of lung metastatic tumors (left) and the number of metastatic tumor nodules (right) (C). Representative flow plots (left) and quantification (right) of IFN-γ$^+$ (D) and CD107a$^+$ (E) cells in NK cells after *ex vivo* stimulation with cell stimulation cocktail.

(F) Quantitative PCR analysis of gDNA and mtDNA in MC38-tdTomato cells sorted from the lung on day 3 after intravenous tumor injection (n = 5 technical replicates from 4 mice).

(G) B16F10 (B16) or 50 μM ddC-treated B16F10 (B16 + ddC) cells were intravenously injected into WT mice (n = 4). Representative appearance of lung metastatic tumors (left) and the number of metastatic tumor nodules (right). Representative data are shown from two or three independent experiments. Data are represented as mean ± SEM. ***p < 0.001, ****p < 0.0001 by unpaired Student's t test. ns, no significant difference. See also Figure S3 and Table S1.

in cultured tumor cells *in vitro*, while no difference was detected between groups in cytosolic gDNA markers (Figure 3F). To further verify the role of mtDNA in tumor metastasis, we depleted mtDNA of B16F10 with dideoxycytidine (ddC) according to a well-established protocol.[1] The ddC treatment selectively inhibited mtDNA replication without affecting gDNA replication in tumor cells (Figure S3D). The number of metastatic tumor nodules was increased in mtDNA-depleted tumor cells compared with that in untreated tumor cells (Figure 3G). Taken together, these results suggest that mtDNA release into the cytosol and subsequent recognition by cGAS in tumor cells sustain the antitumor activity of NK cells.

STING maintains a reservoir of TCF-1$^+$ NK cells in tumors

TCF-1$^+$ NK cell population has been linked with persistent NK cell responses.[24,36] Among the functional markers of differentiation, TCF-1 expression is particularly informative because it is high in immature (CD27$^+$CD11b$^-$) NK cells with elevated proliferative potential, reduced in intermediate (CD27$^+$CD11b$^+$) NK cells, and essentially absent in terminally mature (CD27$^-$CD11b$^+$) NK cells that are poorly proliferative.[25] TCF-1 expression and transcription in the whole-tumor-infiltrating NK cells were diminished in the absence of STING (Figures 4A and S4A), thus indicating that STING signaling associates with the proliferative potential of tumor-infiltrating NK cells. Likewise, we observed a decreased TCF-1 expression in the immature (CD27$^+$CD11b$^-$) NK cell subset of Ncr1^{iCre}STING$^{f/f}$ mice compared with STING$^{f/f}$ controls (Figure 4B). Together, these results indicate that STING serves as an intrinsic factor responsible for maintaining a reservoir of TCF-1$^+$ NK cells in the tumor microenvironment, thereby promoting persistent antitumor responses.

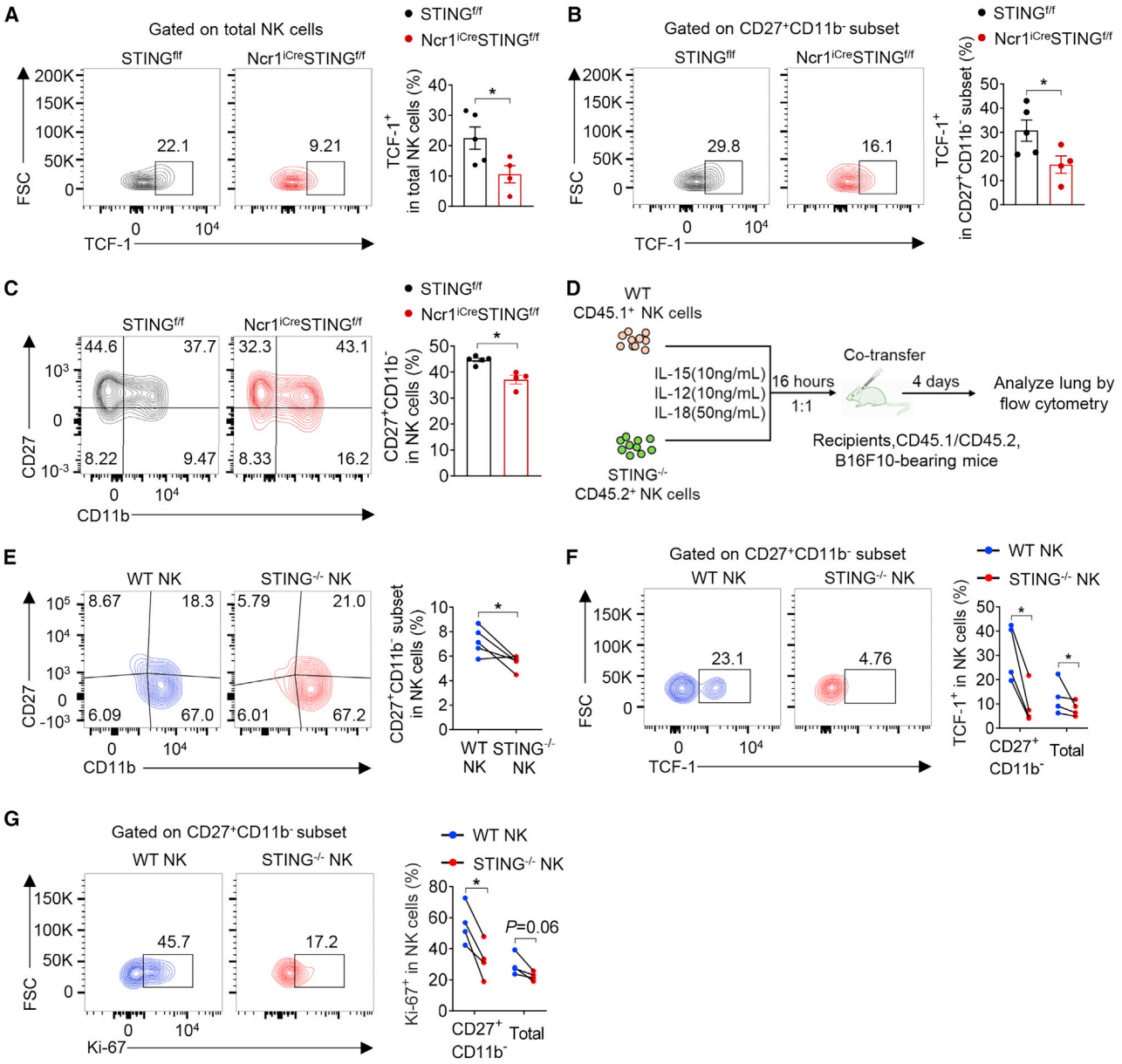

Figure 4. Cell-intrinsic STING facilitates the maintenance of TCF-1$^+$ NK cells in tumors

(A–C) MC38-B2M$^{-/-}$ cells (5 × 10^5) were injected subcutaneously into STING$^{f/f}$ and Ncr1^{iCre}STING$^{f/f}$ mice, respectively (n = 4–5 mice). Tumors were harvested and stained for flow cytometry on day 14 after injection. Representative flow plots (left) and quantification (right) of TCF-1$^+$ cells in total NK cells (A) and CD27$^+$CD11b$^-$ NK cell subset (B) from the subcutaneous tumors. Representative flow plots (left) and quantification (right) of surface CD27/CD11b staining (C) by percentage on intra-tumoral NK cells.

(D) Schematic of WT NK and STING$^{-/-}$ NK cell co-transfer. B16F10 tumor cells (8 × 10^5) were injected into tail vein of WT mice (n = 4–5). One hour later, WT NK and STING$^{-/-}$ NK cells which were labeled with CTV and pre-activated with IL-12/15/18 for 16 h were mixed at a ratio of 1:1 and then co-transferred into tumor-bearing mice. Lungs were analyzed with flow cytometry after 4 days.

(E) Representative flow plots (left) and quantification (right) of the percentage of CD27$^+$CD11b$^-$ (immature) subset in the transferred WT and STING$^{-/-}$ NK cells from the lung of recipients (n = 5) with metastatic B16F10 tumors.

(F) Representative flow plots (left) and quantification (right) of the percentage of TCF-1$^+$ cells in CD27$^+$CD11b$^-$ subset and the total populations in the transferred WT and STING$^{-/-}$ NK cells from the lung of recipients (n = 4) with metastatic B16F10 tumors.

(G) Representative flow plots (left) and quantification (right) of the percentage of Ki-67$^+$ cells in CD27$^+$CD11b$^-$ subset and the total populations in the transferred WT and STING$^{-/-}$ NK cells from the lung of recipients (n = 4) with metastatic B16F10 tumors. Representative data are shown from two or three independent experiments. Data are represented as mean ± SEM. *p < 0.05 by unpaired Student's t test in (A–C), and paired Student's t test in (E–G). See also Figure S4.

The differentiation and maturation of NK cells involve the acquisition of an effector cell program characterized by transient upregulation of CD27 followed by upregulation of CD11b.[36,37] To assess whether STING contributes to expansion of tumor-infiltrating immature NK cells, we injected tumor cells into STING$^{f/f}$ and Ncr1^{iCre}STING$^{f/f}$ mice and quantified the proportions of different NK cell subsets by flow cytometry. The results showed that loss of STING led to a decrease in immature NK cells (CD27$^+$CD11b$^-$) possessing self-renewal capacity (Figure 4C), indicating that STING may promote the expansion of proliferative NK cells in the tumor microenvironment. To investigate whether the STING pathway empowers the expansion of the immature NK cell subset, we simultaneously examined TCF-1 and STING expression in the indicated NK cell subsets from spleen of WT naive mice. We found that both TCF-1 and STING were highly expressed in the immature NK cell subset (Figure S4B). However, the subsets and TCF-1 expression of NK cells in lungs and spleens were unaffected by the deficiency of STING in NK cells (Figures S4C and S4D). Based on the above findings, the impacts of STING on the expansion of TCF-1$^+$ NK cells are restricted to tumors, possibly due to the presence of cGAMP in the tumor microenvironment. These results indicate that immature NK cells in tumors are more responsive to STING stimulation compared with mature NK cells, leading to the expansion of immature TCF-1$^+$ NK cells.

TCF-1$^+$ memory-like NK cells exhibit persistent responses to lymphomas and human immunodeficiency virus 1 infection.[24,28] The expansion of memory-like NK cells can be induced by stimulation with a cytokine cocktail that includes IL-12, IL-15, and IL-18.[26] To determine whether STING signaling is also required for the expansion of the TCF-1$^+$ NK cell population in a therapeutic context, we co-transferred NK cells from WT and STING$^{-/-}$ mice at a ratio of 1:1 after pre-activation with IL-12, IL-15, and IL-18 into metastatic tumor-bearing mice (see experimental schematic in Figures 4D and S4E). To rule out the possibility that STING directly impacts on NK cell responses to the cytokine cocktail stimulation, we analyzed NK cell phenotypes by flow cytometry with staining of CD27, CD11b, and CD69 *in vitro*. The degree of differentiation and activation was comparable between WT-NK cells and STING$^{-/-}$ NK cells upon cytokine stimulation before transfer (Figures S4F and S4G). Loss of STING did not appear to affect the accumulation of adoptively transferred NK cells in the lung of tumor-bearing recipients at 4 days after co-transfer (Figure S4H), indicating that STING does not contribute to the short-term expansion of NK cells in tumors.

To clarify whether STING potentiates the expansion of an immature subset in adoptively transferred NK cells, we used the CD27 and CD11b surface markers and the TCF-1 transcription factor to examine NK cell maturation and differentiation. We found that the frequency of immature (CD27$^+$CD11b$^-$) NK cells was decreased among the adoptively transferred tumor-infiltrating STING$^{-/-}$ NK cells compared with counterpart WT NK cells (Figure 4E). TCF-1 expression has been shown to promote NK cell development, while its downregulation leads to terminal maturation.[25] We found that the proportion of TCF-1$^+$ NK cells was decreased in the tumor-infiltrating immature NK cell subset (indicated as CD27$^+$CD11b$^-$) and total NK cells in the absence of STING (Figures 4F and S4I). Similarly, Ki-67 staining showed that proliferative potential was impaired in the tumor-infiltrating immature NK cell subset with the deficiency of STING (Figures 4G and S4J). In contrast, the progenitor phenotypes and proliferative potential were unaffected by STING deficiency in adoptively transferred NK cells in spleens (Figures S4K–S4M). In addition, a lower expression of Ki-67 and TCF-1 was observed in adoptively transferred STING$^{-/-}$ NK cells compared with counterpart WT-NK cells in tumors 7 days later after co-transfer (Figure S4N), suggesting that the impaired expansion of NK cells induced by STING deficiency occurs in a longer time. Furthermore, we found cGAS loss in tumor cells led to reduced TCF-1$^+$ proportion in the immature NK cell subset and total NK cells from tumors (Figure S4O), confirming that the impacts of STING on expansion of the TCF-1$^+$ NK subset were restricted to tumors because of the presence of tumor-derived cGAMP. Collectively, these results indicate that cell-intrinsic STING signaling promotes the expansion of TCF-1$^+$ NK cells through increased proliferation rather than differentiation or TCF-1 expression, thereby leading to prolonged antitumor responses.

STING agonism enhances NK cell activation via autocrine type I IFN signaling *in vitro*

We next examined whether the incubation of cGAMP could impact on STING signaling, and found that STING expression and transcription were increased by stimulation with cGAMP (Figures S5A and S5B). We next investigated whether cGAMP incubation could prime the activation of STING signaling in NK cells from PBMCs of patients with cancer, and noted that treatment with high concentrations (5 μM) of cGAMP could induce the phosphorylation of STING in NK cells of patients with cancer (Figure 5A), indicating the activation of STING signaling in NK cells. Consistently, the activation of the STING pathway was observed in NK-92MI cell line with the stimulation of cGAMP (Figure 5B). To investigate whether the entry of exogenous cGAMP directly activates NK cells through involving STING, we treated WT and STING$^{-/-}$ NK cells with different concentrations of 2′3′-cGAMP *in vitro* and quantified NK cell activation by CD69 staining. The results showed that CD69 expression was increased following incubation with high concentrations (5 μM) of cGAMP, whereas the observed upregulation of CD69 in NK cells was abolished under STING knockout (Figures 5C and S5C). These results suggest that NK cells could uptake cGAMP, which in turn primes STING signaling, thus leading to NK cell activation.

To better understand the molecular machinery underlying the effects of intrinsic STING signaling in NK cells, we purified NK cells from the spleens of WT naive mice by flow cytometric cell sorting and quantified IFN-β production by NK cells incubated with cGAMP (Figure S5D). Indeed, exposure to exogenous cGAMP could induce the production of *Ifnb1* and IFN-stimulated gene (*Cxcl10*, *Irf7*, and *Isg15*) transcription in NK cells (Figures 5D and S5E). Moreover, the elevated activation of NK cells after incubation with cGAMP was reversed by the blockade of IFNAR1 (Figure 5E). Specifically, IFNAR1 loss in NK cells dampened NK cell activation upon cGAMP exposure (Figures 5F and S5F). These results suggest that cGAMP treatment promotes NK cell activation via autocrine type I IFN signaling *in vitro*.

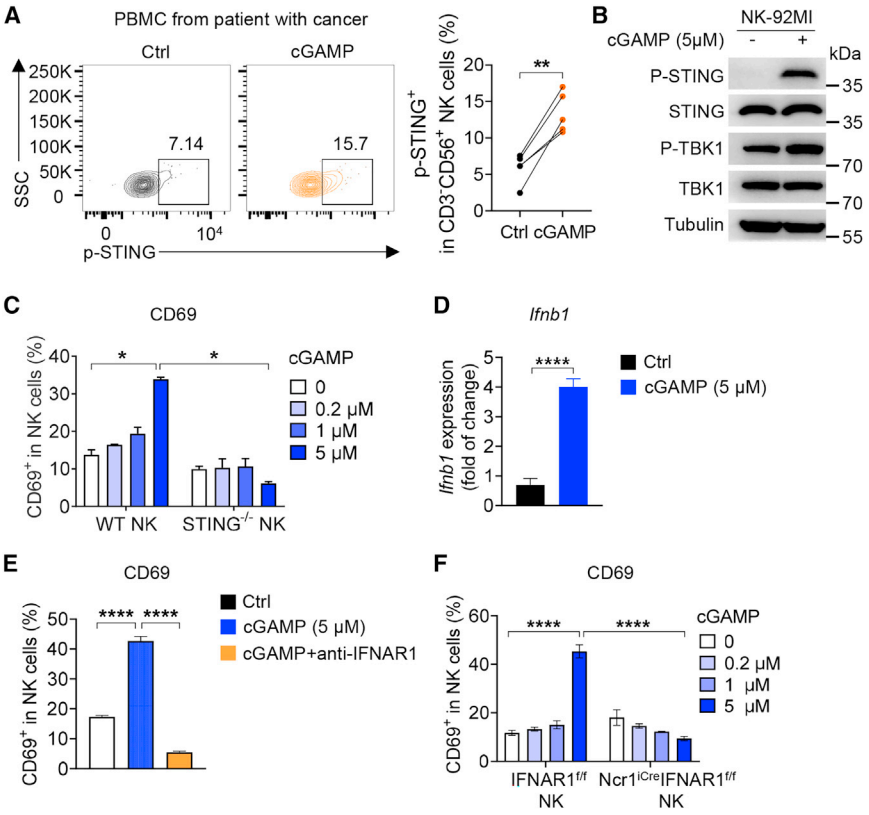

Figure 5. STING agonism enhances NK cell activation *in vitro*

(A) Representative flow plots (left) and quantitative data (right) of p-STING^{S336} expression in NK cells from PBMCs of patients with cancer stimulated with or without cGAMP (5 μM) for 4 h. Each dot represents one patient (n = 5, Table S2, patients 24–28).

(B) Western blot showing p-STING and p-TBK1 expression in NK-92MI cell lines after cGAMP (5 μM) treatment for 6 h.

(C) Quantification of CD69 expression in WT and STING$^{-/-}$ NK cells stimulated with different concentrations of cGAMP as indicated (0, 0.2, 1, and 5 μM) in the presence of hIL-15 (10 ng/mL) (n = 3 replicates).

(D) Quantification of *Ifnb1* mRNA expression in NK cells stimulated with or without cGAMP (5 μM) in the presence of hIL-15 (10 ng/mL) (n = 4 replicates).

(E) Quantification of CD69 expression in NK cells stimulated with cGAMP in the presence or absence of anti-IFNAR1 antibody (200 μg/ml) (n = 3 replicates).

(F) Quantification of CD69 expression in IFNAR1$^{f/f}$ and Ncr1^{iCre}IFNAR1$^{f/f}$ NK cells stimulated with different concentrations of cGAMP as indicated (0, 0.2, 1, and 5 μM) in the presence of hIL-15 (10 ng/mL) (n = 3 replicates). Representative data are shown from two or three independent experiments. Data are represented as mean ± SEM. *p < 0.05, **p < 0.01, ****p < 0.0001 by paired Student's t test in (A), one-way ANOVA in (C, E, and F), and unpaired Student's t test in (D). See also Figure S5; Tables S1 and S2.

STING agonism facilitates the expansion of TCF-1$^+$ NK cells in humans

Previous studies have demonstrated that TCF-1 is associated with the memory-like status of NK cells in humans.[24,36] We found that the expression level of TCF-1 was decreased in CD3$^-$CD56$^+$ NK cells in the peripheral blood samples of patients with cancer compared with that of healthy volunteers (Figure 6A), which suggested that the maintenance of memory-like status was disrupted in NK cells of patients with cancer. We therefore investigated whether STING was associated with the maintenance of TCF-1$^+$ NK cells by quantification of STING expression in different NK cell subsets. We found that STING expression was higher in TCF-1$^+$ NK cells than that in the TCF-1$^-$ NK cells from PBMCs of patients with cancer and healthy volunteers (Figures 6B and S6A), thus revealing a positive correlation between STING expression and the proportion of TCF-1$^+$ NK cells. Furthermore, to delineate TCF-1 and STING expression level in human NK cells at different stages of maturation we examined expression of both molecules in CD56^{dim} and CD56^{hi} NK cells from PBMCs of patients with cancer and healthy volunteers. Consistent with our observation in mouse NK cells, immature CD56^{hi} NK cells exhibited a higher expression level of TCF-1 and STING in human settings (Figures S6B and S6C). These lines of evidence imply that STING signaling associates with the expansion of TCF-1$^+$ NK cells in humans.

Cytokine-induced memory-like NK cells exhibit more potent antitumor activity with the stimulation of IL-12, IL-15, and IL-18.[28] NK cell function also correlates with CD56 expression; following IL-15 priming, immature CD56$^+$ NK cells exhibited elevated expansion, cytokine production, and antitumor responses.[30] Given that boosting the STING pathway could potentiate the expansion of TCF-1$^+$ NK cells in mouse tumor models, we next examined whether prolonged incubation with cGAMP could potentiate the maintenance of immature human CD56$^+$ NK cells. To this end, human NK cells were purified and pre-activated with IL-15 for 16 h and the cells were then incubated with low concentrations (1 μM) of cGAMP plus IL-15 for 7 days (see experimental scheme in Figures 6C and S6D). We found that prolonged exposure to the combination of cGAMP and IL-15 could increase the proportion of immature CD56^{hi}CD16$^-$ NK cells, while decreasing the proportion of CD16$^+$ NK cells when compared with IL-15 alone (Figure S6E). Notably, CD56 expression on CD16$^+$CD56^{dim} NK cells was increased by the stimulation of cGAMP and IL-15 (Figure S6E). Consistently, such observations were also reported in other study.[38] Meanwhile, we assessed TCF-1 expression in total CD56$^+$ NK cells and found that the percentages of TCF-1$^+$ NK cells were increased by the combination treatment of cGAMP and IL-15 compared with IL-15 treatment alone (Figure 6D). Also, Ki-67 expression was higher in the TCF-1$^+$ NK subset than that in the TCF-1$^-$ NK subset upon cGAMP treatment (Figure S6F), suggesting a stronger

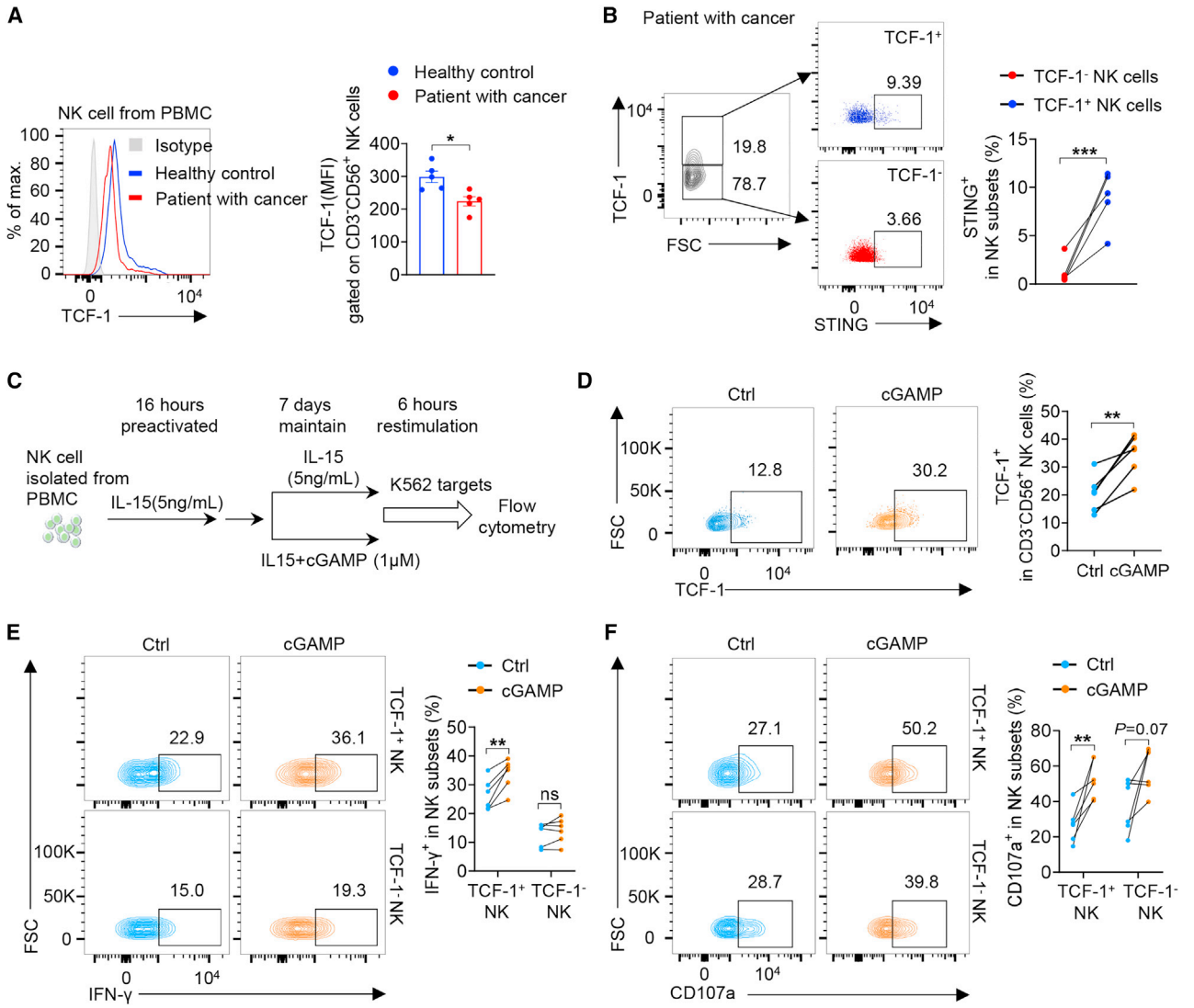

Figure 6. STING agonism promotes the maintenance and function of human immature NK cells

(A) Representative flow plots (left) and quantitative data (right) showing TCF-1 expression in NK cells from peripheral blood of healthy control and patients with cancer (n = 5, Table S2, patients 24–28).

(B) Representative flow plots (left) and quantitative data (right) showing STING expression in TCF-1$^+$ and TCF-1$^-$ NK cells from peripheral blood of patients with cancer (n = 5, Table S2, patients 24–28).

(C) Effect of cGAMP on the expansion and function of human NK cells. Experimental schematic for the generation of memory-like NK cells derived from peripheral blood of healthy volunteers (n = 6).

(D) Representative flow plots (left) and quantitative data (right) of TCF-1$^+$ NK cells after stimulated with IL-15 with or without cGAMP (1 μM) maintenance for 7 days.

(E and F) Representative flow plots (left) and quantitative data (right) of IFN-γ$^+$ NK cells (E) and CD107a$^+$ NK cells (F) in TCF-1$^+$ NK and TCF-1$^-$ NK subsets in response to re-stimulation with K562 cells after treatment with IL-15 with or without cGAMP (1 μM) maintenance for 7 days. Data are represented as mean ± SEM. *p < 0.05, **p < 0.01, ***p < 0.001 by unpaired Student's t test in (A), and paired Student's t test in (B and D–F). ns, no significant difference. See also Figure S6 and Table S2.

proliferation potential in the TCF-1$^+$ NK subset. Moreover, the expressions of IFN-γ and CD107a were increased in the TCF-1$^+$ NK cell subset in response to restimulation with K562 leukemia cells 7 days following cGAMP treatment compared with control treatment (Figures 6E and 6F), indicating that STING agonism increases the responsiveness of the TCF-1$^+$ NK cell subset that leads to IFN-γ and CD107a production. Collectively, these results suggest that STING agonism facilitates the expansion and function of immature TCF1$^+$ NK cells, and that cGAMP treatment may be used to broaden the application of NK cell-based therapeutics.

DISCUSSION

The role of innate immune sensing in regulating cytotoxic lymphocytes is the focus of considerable research attention seeking

to exploit their therapeutic potential for improved antitumor immune response. Our study demonstrates that the cGAS-STING cascade serves as a form of direct communication between tumor cells and NK cells via intercellular transfer of cGAMP from the former to the latter. STING functions as an intrinsic regulator of potent effector functions and maintenance of TCF-1$^+$ NK cells in tumors. It is conceivable that aberrant STING expression in NK cells may participate in tumor immune evasion, while STING agonism reinvigorates NK cell antitumor activity. Our findings thus expand the scope of our understanding of STING functions in the antitumor activity of NK cells and point to viable therapeutic strategies for the expansion of TCF-1$^+$ NK cells.

Considering the potential value of STING for clinical translation, the mechanisms and effects of intrinsic STING signaling have been intensively studied in different cell types ranging from tumor cells and antigen-presenting cells to cytotoxic immune cells. First, the cGAS-STING pathway contributes to tumor immunogenicity by bridging DNA damage response signals to host antitumor immunity in the context of PARP inhibitor treatment and radiotherapy.[1,4,10–12] Second, the cGAS-STING pathway initiates the process of cross-priming by dendritic cells in responses to tumor radiotherapy and immunotherapy.[2,3] Third, the cGAS-STING pathway maintains the differentiation of stem cell-like CD8$^+$ T cells to activate a durable antitumor immune response.[13] Our findings provide further perspective on STING function in antitumor immunity. In particular, we found that STING promotes effector functions and preservation of TCF-1$^+$ NK cells for successful tumor surveillance. However, whether other immune cell dependency in this process needs further investigations. Based on these findings, it is reasonable to speculate that abnormally low STING expression in NK cells can serve as a major contributing factor that leads to tumor immune evasion, and further work is needed to determine which factors in the tumor microenvironment can lead to the downregulation of STING in NK cells. Given the potential for STING agonism as a therapeutic strategy for cancer,[8] the direct impacts of STING agonists on NK cells also warrants careful evaluation in clinical trials.

In response to cellular stress, cGAS is critical for recognition of cytosolic DNA and subsequent activation of an innate immune response.[10–12,39,40] However, initiation of the cGAS-STING cascade often involves intercellular transfer of cGAMP between two different cell types, presumably mediated by gap junction, volume-regulated anion channels and other transporters including SLC19A1 and SLC46A2.[35,41–45] Moreover, P2X7R engagement contributes to cGAMP entry into tumor-associated macrophages after blockade of the phagocytic receptor MerTK.[46] We found that cGAS in tumor cells, rather than in host cells, promotes the antitumor activity of NK cells, which is consistent with the results from another report.[31] Moreover, our results indicate that the intercellular transfer of cGAMP from tumor cells to NK cells is responsible for NK cell response toward tumor cells. Indeed, incubation with cGAMP enhances NK cell activation in both mice and humans, validating the possibility that cGAMP originates by intercellular transfer. In addition, we observed that cytoplasmic mtDNA is enriched in metastatic MC38 tumor cells and that depletion of mtDNA augments tumor metastasis, indicating that recognition of mtDNA initiates the production of cGAMP in tumor cells. However, we do not validate how general this phenomenon is. It is possible that genomic DNA may play a key role in other tumors, including natural primary tumors. BAK/BAX macropores then facilitate mtDNA leakage in apoptotic cells, while voltage-dependent anion channel oligomers promote mtDNA release in live cells by forming mitochondrial pores.[39,40,47,48] In addition, further studies are needed to address how mtDNA is released in metastatic tumor cells.

A previous study has shown that STING activation could initiate the downstream activation of the transcription factors IFN regulatory factor 3 and nuclear factor κB and further lead to production of various cytokines and chemokines, especially type I IFNs.[9] Our results showed exogenous cGAMP treatment could promote NK cell activation via autocrine type I IFN signal *in vitro*, suggesting the direct action of type I IFN on NK cells, which is consistent with the observation that type I IFNs could directly act on NK cell antitumor activity after cyclic dinucleotide treatment *in vivo*.[7] Considering that *in vitro* stimulations may not recapitulate *in vivo* conditions, we acknowledge that the necessary amount of type I IFN *in vivo* may come from other cells besides NK cells. Therefore, future experiments will examine the molecular mechanisms underlying STING-mediated maintenance of TCF-1$^+$ NK cell response in the tumor contexture.

The modification of NK cells with CAR has been considered a viable alternative to T cells in cancer therapy.[17,19] However, establishing a means of inducing a persistent response in infused CAR-NK cells remains a major obstacle for clinical application. We found that STING signaling promotes effector functions and expansion of immature TCF-1$^+$ NK cells in tumors. Many other studies have reported that TCF-1$^+$ NK cells show the same transcriptional and epigenetic characters with the stem-like exhausted CD8$^+$ T cells,[24,49,50] and IL-12/15/18-preactivate or cytokine-induced memory-like NK cells show potential for cancer immunotherapy in the clinic.[51–53] TCF-1 is required for the maintenance for memory-like NK cells, which exhibit enhanced functional responses.[24] Thus, the STING agonist may function as a stimulator for preservation of memory-like state in adoptive NK cell therapy.

Human NK cells are widely divided into cytotoxic CD56^{dim} CD16$^+$ NK cells and cytokine secreting CD56^{hi}CD16$^-$ NK cells.[29] Also, the NK1 transcriptomic profile corresponds to human CD56^{dim} and mouse CD27$^-$CD11b$^+$ NK cells and the NK2 transcriptomic profile corresponds to human CD56^{hi} and mouse CD27$^+$CD11b$^-$ NK cells.[54] We found that STING and TCF-1 expression were much higher in immature CD27$^+$CD11b$^-$ NK subsets of mice and in CD56^{hi} NK cells of humans. These results suggest that immature TCF-1$^+$ NK cells are more responsive to STING stimulation compared with mature NK cells. Given that the developmental defect of NK cells in Ncr1^{iCre}Id2$^{f/f}$ mice, the increased TCF-1 expression in ID2-deficient NK cells arrests their maturation and inhibits their functions.[55] In contrast, TCF-1 expression positively associates with NK cell functions in our settings due to the normal development of NK cells in Ncr1^{iCre}STING$^{f/f}$ mice. To reconcile the inconsistence, we assume that TCF-1 may play a dichotomous role in NK cells. Constitutive ectopic expression of TCF-1 in NK cells with developmental defects inhibits NK cell functions, whereas inducible

expression of TCF-1 in NK cells with normal development promotes NK cell antitumor activity. In addition, intrinsic STING signaling may affect TCF-1 expression through promoting the expansion of immature TCF-1$^+$ NK cells rather than directly regulating its transcriptome in NK cells. However, considering that TCF-1 could bind to a substantial set of genes in CD27$^+$CD11b$^-$ NK cells,[55–57] TCF-1 expression in tumor-infiltrating NK cells might correlate with some other cellular properties that result in better antitumor responses. Thus, it is likely that the opposite impact of TCF-1 on NK cell functions may be observed in the different settings. In PBMCs, CD56^{hi} NK cells as a potent cytokine producers exhibit better antitumor responses than CD56^{dim} NK cells following IL-15 priming.[30] In line with these results, extended incubation with cGAMP induced the expansion of human CD56^{hi} NK cells and higher levels of IFN-γ and CD107a *in vitro*. Thus, regulation of CD56^{hi} NK cells can improve their antitumor functions and be a potent cancer immunotherapy. However, further *in vivo* studies with xenograft models or in patients are needed to validate the initial observation described here.

Overall, our data provide a plausible explanation for the mechanisms by which NK cells conduct tumor surveillance, and uncover new insights into STING functions in antitumor immunity. We also propose that augmentation of STING pathway activation in NK cells can substantially broaden their application in cancer therapies.

Limitations of the study

Our study does have certain limitations, such as the molecular mechanism of cGAMP transfer into NK cells in tumor niches. How inherent STING signaling promotes the expansion of TCF-1$^+$ NK in tumors needs to be further determined. In addition, we demonstrated upregulation of CD69 in NK cells after cGAMP stimulation *in vitro* is dependent on autocrine type I IFN signal; however, it is not clear whether NK cells are the critical source of type I IFN induced by cGAMP *in vivo* conditions. Although we found that STING agonist facilitates the expansion of TCF-1$^+$ NK cells *in vitro*, whether human CAR-NK cells pretreated with STING agonist have a better antitumor response *in vivo* needs further investigation.

STAR★METHODS

Detailed methods are provided in the online version of this paper and include the following:

SUPPLEMENTAL INFORMATION

Supplemental information can be found online at https://doi.org/10.1016/j.celrep.2023.113108.

ACKNOWLEDGMENTS

BioRender was used for the graphical abstract. We gratefully acknowledge Junke Zheng for helpful scientific discussion and assistance. We thank the Flow Cytometry Facility and Animal Resources Center of Shanghai Jiao Tong University and Shanghai Jiao Tong University School of Medicine. Funding: National Natural Science Foundation of China (81771682 and 82071741 to L.D., 32100731 to L.L.), National Thousand Youth Talents Program (to L.D.), National Key R&D Program of China (2020YFA0210800), Science and Technology Commission of Shanghai Municipality (16JC1406000 to L.D.), Fundamental Research Funds for the Central Universities and Interdisciplinary Program of Shanghai Jiao Tong University (YG2021ZD03 to L.D.), New Teacher Initiation Program of Shanghai Jiao Tong University (22X010500258 to L.L.), and Open grant of Shanghai Key Laboratory of Gynecologic Oncology at Ren Ji Hospital (FKZL-2021-01 to L.L.).

AUTHOR CONTRIBUTIONS

L.L. and C.Y. performed the experiments and wrote original draft. X.Z. contributed to part of the revised data. L.W., X.H., and W.L. aided in the experiments of real-time PCR and part of *in vitro* analysis. X.W. aided in the experiments of flow cytometry assay. Y.Y. and D.C. aided in some experiments of real-time PCR and western blot. L.L., C.Y., W.L., and A.Z. analyzed the data. W.D. provided the samples from patients with cancer. L.D. conceived and supervised all experiments and writing the manuscript.

DECLARATION OF INTERESTS

L.L., C.Y., and L.D. have filed a patent application related to this project.

Received: November 17, 2022
Revised: August 3, 2023
Accepted: August 24, 2023
Published: September 13, 2023

REFERENCES

1. Yang, Y., Wu, M., Cao, D., Yang, C., Jin, J., Wu, L., Hong, X., Li, W., Lu, L., Li, J., et al. (2021). ZBP1-MLKL necroptotic signaling potentiates radiation-induced antitumor immunity via intratumoral STING pathway activation. Sci. Adv. *7*, eabf6290. https://doi.org/10.1126/sciadv.abf6290.
2. Deng, L., Liang, H., Xu, M., Yang, X., Burnette, B., Arina, A., Li, X.D., Mauceri, H., Beckett, M., Darga, T., et al. (2014). STING-Dependent Cytosolic DNA Sensing Promotes Radiation-Induced Type I Interferon-Dependent Antitumor Immunity in Immunogenic Tumors. Immunity *41*, 843–852. https://doi.org/10.1016/j.immuni.2014.10.019.
3. Xu, M.M., Pu, Y., Han, D., Shi, Y., Cao, X., Liang, H., Chen, X., Li, X.D., Deng, L., Chen, Z.J., et al. (2017). Dendritic Cells but Not Macrophages Sense Tumor Mitochondrial DNA for Cross-priming through Signal

Regulatory Protein α Signaling. Immunity *47*, 363–373.e5. https://doi.org/10.1016/j.immuni.2017.07.016.

4. Pantelidou, C., Sonzogni, O., De Oliveria Taveira, M., Mehta, A.K., Kothari, A., Wang, D., Visal, T., Li, M.K., Pinto, J., Castrillon, J.A., et al. (2019). PARP Inhibitor Efficacy Depends on CD8(+) T-cell Recruitment via Intratumoral STING Pathway Activation in BRCA-Deficient Models of Triple-Negative Breast Cancer. Cancer Discov. *9*, 722–737. https://doi.org/10.1158/2159-8290.Cd-18-1218.
5. Demaria, O., Cornen, S., Daëron, M., Morel, Y., Medzhitov, R., and Vivier, E. (2019). Harnessing innate immunity in cancer therapy. Nature *574*, 45–56. https://doi.org/10.1038/s41586-019-1593-5.
6. McLaughlin, M., Patin, E.C., Pedersen, M., Wilkins, A., Dillon, M.T., Melcher, A.A., and Harrington, K.J. (2020). Inflammatory microenvironment remodelling by tumour cells after radiotherapy. Nat. Rev. Cancer *20*, 203–217. https://doi.org/10.1038/s41568-020-0246-1.
7. Nicolai, C.J., Wolf, N., Chang, I.C., Kirn, G., Marcus, A., Ndubaku, C.O., McWhirter, S.M., and Raulet, D.H. (2020). NK cells mediate clearance of CD8 T cell-resistant tumors in response to STING agonists. Sci. Immunol. *5*, eaaz2738. https://doi.org/10.1126/sciimmunol.aaz2738.
8. McWhirter, S.M., and Jefferies, C.A. (2020). Nucleic Acid Sensors as Therapeutic Targets for Human Disease. Immunity *53*, 78–97. https://doi.org/10.1016/j.immuni.2020.04.004.
9. Kwon, J., and Bakhoum, S.F. (2020). The Cytosolic DNA-Sensing cGAS-STING Pathway in Cancer. Cancer Discov. *10*, 26–39. https://doi.org/10.1158/2159-8290.CD-19-0761.
10. Dou, Z., Ghosh, K., Vizioli, M.G., Zhu, J., Sen, P., Wangensteen, K.J., Simithy, J., Lan, Y., Lin, Y., Zhou, Z., et al. (2017). Cytoplasmic chromatin triggers inflammation in senescence and cancer. Nature *550*, 402–406. https://doi.org/10.1038/nature24050.
11. Harding, S.M., Benci, J.L., Irianto, J., Discher, D.E., Minn, A.J., and Greenberg, R.A. (2017). Mitotic progression following DNA damage enables pattern recognition within micronuclei. Nature *548*, 466–470. https://doi.org/10.1038/nature23470.
12. Mackenzie, K.J., Carroll, P., Martin, C.A., Murina, O., Fluteau, A., Simpson, D.J., Olova, N., Sutcliffe, H., Rainger, J.K., Leitch, A., et al. (2017). cGAS surveillance of micronuclei links genome instability to innate immunity. Nature *548*, 461–465. https://doi.org/10.1038/nature23449.
13. Li, W., Lu, L., Lu, J., Wang, X., Yang, C., Jin, J., Wu, L., Hong, X., Li, F., Cao, D., et al. (2020). cGAS-STING-mediated DNA sensing maintains CD8(+) T cell stemness and promotes antitumor T cell therapy. Sci. Transl. Med. *12*, eaay9013. https://doi.org/10.1126/scitranslmed.aay9013.
14. Morvan, M.G., and Lanier, L.L. (2016). NK cells and cancer: you can teach innate cells new tricks. Nat. Rev. Cancer *16*, 7–19. https://doi.org/10.1038/nrc.2015.5.
15. López-Soto, A., Gonzalez, S., Smyth, M.J., and Galluzzi, L. (2017). Control of Metastasis by NK Cells. Cancer Cell *32*, 135–154. https://doi.org/10.1016/j.ccell.2017.06.009.
16. Bald, T., Krummel, M.F., Smyth, M.J., and Barry, K.C. (2020). The NK cell-cancer cycle: advances and new challenges in NK cell-based immunotherapies. Nat. Immunol. *21*, 835–847. https://doi.org/10.1038/s41590-020-0728-z.
17. Huntington, N.D., Cursons, J., and Rautela, J. (2020). The cancer-natural killer cell immunity cycle. Nat. Rev. Cancer *20*, 437–454. https://doi.org/10.1038/s41568-020-0272-z.
18. Myers, J.A., and Miller, J.S. (2021). Exploring the NK cell platform for cancer immunotherapy. Nat. Rev. Clin. Oncol. *18*, 85–100. https://doi.org/10.1038/s41571-020-0426-7.
19. Shimasaki, N., Jain, A., and Campana, D. (2020). NK cells for cancer immunotherapy. Nat. Rev. Drug Discov. *19*, 200–218. https://doi.org/10.1038/s41573-019-0052-1.
20. Zemek, R.M., De Jong, E., Chin, W.L., Schuster, I.S., Fear, V.S., Casey, T.H., Forbes, C., Dart, S.J., Leslie, C., Zaitouny, A., et al. (2019). Sensitization to immune checkpoint blockade through activation of a STAT1/NK axis in the tumor microenvironment. Sci. Transl. Med. *11*, eaav7816. https://doi.org/10.1126/scitranslmed.aav7816.
21. O'Sullivan, T.E., Sun, J.C., and Lanier, L.L. (2015). Natural Killer Cell Memory. Immunity *43*, 634–645. https://doi.org/10.1016/j.immuni.2015.09.013.
22. Fehniger, T.A., and Cooper, M.A. (2016). Harnessing NK Cell Memory for Cancer Immunotherapy. Trends Immunol. *37*, 877–888. https://doi.org/10.1016/j.it.2016.09.005.
23. Cerwenka, A., and Lanier, L.L. (2016). Natural killer cell memory in infection, inflammation and cancer. Nat. Rev. Immunol. *16*, 112–123. https://doi.org/10.1038/nri.2015.9.
24. Wang, Y., Lifshitz, L., Gellatly, K., Vinton, C.L., Busman-Sahay, K., McCauley, S., Vangala, P., Kim, K., Derr, A., Jaiswal, S., et al. (2020). HIV-1-induced cytokines deplete homeostatic innate lymphoid cells and expand TCF7-dependent memory NK cells. Nat. Immunol. *21*, 274–286. https://doi.org/10.1038/s41590-020-0593-9.
25. Jeevan-Raj, B., Gehrig, J., Charmoy, M., Chennupati, V., Grandclément, C., Angelino, P., Delorenzi, M., and Held, W. (2017). The Transcription Factor Tcf1 Contributes to Normal NK Cell Development and Function by Limiting the Expression of Granzymes. Cell Rep. *20*, 613–626. https://doi.org/10.1016/j.celrep.2017.06.071.
26. Romee, R., Rosario, M., Berrien-Elliott, M.M., Wagner, J.A., Jewell, B.A., Schappe, T., Leong, J.W., Abdel-Latif, S., Schneider, S.E., Willey, S., et al. (2016). Cytokine-induced memory-like natural killer cells exhibit enhanced responses against myeloid leukemia. Sci. Transl. Med. *8*, 357ra123. https://doi.org/10.1126/scitranslmed.aaf2341.
27. Ni, J., Miller, M., Stojanovic, A., Garbi, N., and Cerwenka, A. (2012). Sustained effector function of IL-12/15/18-preactivated NK cells against established tumors. J. Exp. Med. *209*, 2351–2365. https://doi.org/10.1084/jem.20120944.
28. Gang, M., Marin, N.D., Wong, P., Neal, C.C., Marsala, L., Foster, M., Schappe, T., Meng, W., Tran, J., Schaettler, M., et al. (2020). CAR-modified memory-like NK cells exhibit potent responses to NK-resistant lymphomas. Blood *136*, 2308–2318. https://doi.org/10.1182/blood.2020006619.
29. Caligiuri, M.A. (2008). Human natural killer cells. Blood *112*, 461–469. https://doi.org/10.1182/blood-2007-09-077438.
30. Wagner, J.A., Rosario, M., Romee, R., Berrien-Elliott, M.M., Schneider, S.E., Leong, J.W., Sullivan, R.P., Jewell, B.A., Becker-Hapak, M., Schappe, T., et al. (2017). CD56bright NK cells exhibit potent antitumor responses following IL-15 priming. J. Clin. Invest. *127*, 4042–4058. https://doi.org/10.1172/jci90387.
31. Marcus, A., Mao, A.J., Lensink-Vasan, M., Wang, L., Vance, R.E., and Raulet, D.H. (2018). Tumor-Derived cGAMP Triggers a STING-Mediated Interferon Response in Non-tumor Cells to Activate the NK Cell Response. Immunity *49*, 754–763.e4. https://doi.org/10.1016/j.immuni.2018.09.016.
32. Lam, K.C., Araya, R.E., Huang, A., Chen, Q., Di Modica, M., Rodrigues, R.R., Lopès, A., Johnson, S.B., Schwarz, B., Bohrnsen, E., et al. (2021). Microbiota triggers STING-type I IFN-dependent monocyte reprogramming of the tumor microenvironment. Cell *184*, 5338–5356.e21. https://doi.org/10.1016/j.cell.2021.09.019.
33. Wolf, N.K., Blaj, C., Picton, L.K., Snyder, G., Zhang, L., Nicolai, C.J., Ndubaku, C.O., McWhirter, S.M., Garcia, K.C., and Raulet, D.H. (2022). Synergy of a STING agonist and an IL-2 superkine in cancer immunotherapy against MHC I-deficient and MHC I(+) tumors. Proc. Natl. Acad. Sci. USA *119*, e2200568119. https://doi.org/10.1073/pnas.2200568119.
34. Madera, S., Rapp, M., Firth, M.A., Beilke, J.N., Lanier, L.L., and Sun, J.C. (2016). Type I IFN promotes NK cell expansion during viral infection by protecting NK cells against fratricide. J. Exp. Med. *213*, 225–233. https://doi.org/10.1084/jem.20150712.
35. Cordova, A.F., Ritchie, C., Böhnert, V., and Li, L. (2021). Human SLC46A2 Is the Dominant cGAMP Importer in Extracellular cGAMP-Sensing

Macrophages and Monocytes. ACS Cent. Sci. *7*, 1073–1088. https://doi.org/10.1021/acscentsci.1c00440.

36. Collins, P.L., Cella, M., Porter, S.I., Li, S., Gurewitz, G.L., Hong, H.S., Johnson, R.P., Oltz, E.M., and Colonna, M. (2019). Gene Regulatory Programs Conferring Phenotypic Identities to Human NK Cells. Cell *176*, 348–360.e12. https://doi.org/10.1016/j.cell.2018.11.045.
37. Crinier, A., Narni-Mancinelli, E., Ugolini, S., and Vivier, E. (2020). SnapShot: Natural Killer Cells. Cell *180*, 1280–1280.e1. https://doi.org/10.1016/j.cell.2020.02.029.
38. Keskin, D.B., Allan, D.S.J., Rybalov, B., Andzelm, M.M., Stern, J.N.H., Kopcow, H.D., Koopman, L.A., and Strominger, J.L. (2007). TGFbeta promotes conversion of CD16+ peripheral blood NK cells into CD16- NK cells with similarities to decidual NK cells. Proc. Natl. Acad. Sci. USA *104*, 3378–3383. https://doi.org/10.1073/pnas.0611098104.
39. Rongvaux, A., Jackson, R., Harman, C.C.D., Li, T., West, A.P., de Zoete, M.R., Wu, Y., Yordy, B., Lakhani, S.A., Kuan, C.Y., et al. (2014). Apoptotic caspases prevent the induction of type I interferons by mitochondrial DNA. Cell *159*, 1563–1577. https://doi.org/10.1016/j.cell.2014.11.037.
40. White, M.J., McArthur, K., Metcalf, D., Lane, R.M., Cambier, J.C., Herold, M.J., van Delft, M.F., Bedoui, S., Lessene, G., Ritchie, M.E., et al. (2014). Apoptotic caspases suppress mtDNA-induced STING-mediated type I IFN production. Cell *159*, 1549–1562. https://doi.org/10.1016/j.cell.2014.11.036.
41. Chen, Q., Boire, A., Jin, X., Valiente, M., Er, E.E., Lopez-Soto, A., Jacob, L., Patwa, R., Shah, H., Xu, K., et al. (2016). Carcinoma-astrocyte gap junctions promote brain metastasis by cGAMP transfer. Nature *533*, 493–498. https://doi.org/10.1038/nature18268.
42. Ablasser, A., Schmid-Burgk, J.L., Hemmerling, I., Horvath, G.L., Schmidt, T., Latz, E., and Hornung, V. (2013). Cell intrinsic immunity spreads to bystander cells via the intercellular transfer of cGAMP. Nature *503*, 530–534. https://doi.org/10.1038/nature12640.
43. Zhou, C., Chen, X., Planells-Cases, R., Chu, J., Wang, L., Cao, L., Li, Z., López-Cayuqueo, K.I., Xie, Y., Ye, S., et al. (2020). Transfer of cGAMP into Bystander Cells via LRRC8 Volume-Regulated Anion Channels Augments STING-Mediated Interferon Responses and Anti-viral Immunity. Immunity *52*, 767–781.e6. https://doi.org/10.1016/j.immuni.2020.03.016.
44. Luteijn, R.D., Zaver, S.A., Gowen, B.G., Wyman, S.K., Garelis, N.E., Onia, L., McWhirter, S.M., Katibah, G.E., Corn, J.E., Woodward, J.J., and Raulet, D.H. (2019). SLC19A1 transports immunoreactive cyclic dinucleotides. Nature *573*, 434–438. https://doi.org/10.1038/s41586-019-1553-0.
45. Ritchie, C., Cordova, A.F., Hess, G.T., Bassik, M.C., and Li, L. (2019). SLC19A1 Is an Importer of the Immunotransmitter cGAMP. Mol. Cell *75*, 372–381.e5. https://doi.org/10.1016/j.molcel.2019.05.006.
46. Zhou, Y., Fei, M., Zhang, G., Liang, W.C., Lin, W., Wu, Y., Piskol, R., Ridgway, J., McNamara, E., Huang, H., et al. (2020). Blockade of the Phagocytic Receptor MerTK on Tumor-Associated Macrophages Enhances P2X7R-Dependent STING Activation by Tumor-Derived cGAMP. Immunity *52*, 357–373.e9. https://doi.org/10.1016/j.immuni.2020.01.014.
47. McArthur, K., Whitehead, L.W., Heddleston, J.M., Li, L., Padman, B.S., Oorschot, V., Geoghegan, N.D., Chappaz, S., Davidson, S., San Chin, H., et al. (2018). BAK/BAX macropores facilitate mitochondrial herniation and mtDNA efflux during apoptosis. Science *359*, eaao6047. https://doi.org/10.1126/science.aao6047.
48. Kim, J., Gupta, R., Blanco, L.P., Yang, S., Shteinfer-Kuzmine, A., Wang, K., Zhu, J., Yoon, H.E., Wang, X., Kerkhofs, M., et al. (2019). VDAC oligomers form mitochondrial pores to release mtDNA fragments and promote lupus-like disease. Science *366*, 1531–1536. https://doi.org/10.1126/science.aav4011.
49. Lau, C.M., Adams, N.M., Geary, C.D., Weizman, O.E., Rapp, M., Pritykin, Y., Leslie, C.S., and Sun, J.C. (2018). Epigenetic control of innate and adaptive immune memory. Nat. Immunol. *19*, 963–972. https://doi.org/10.1038/s41590-018-0176-1.
50. Kujur, W., Murillo, O., Adduri, R.S.R., Vankayalapati, R., Konduru, N.V., and Mulik, S. (2020). Memory like NK cells display stem cell like properties after Zika virus infection. PLoS Pathog. *16*, e1009132. https://doi.org/10.1371/journal.ppat.1009132.
51. Terrén, I., Orrantia, A., Astarloa-Pando, G., Amarilla-Irusta, A., Zenarruzabeitia, O., and Borrego, F. (2022). Cytokine-Induced Memory-Like NK Cells: From the Basics to Clinical Applications. Front. Immunol. *13*, 884648. https://doi.org/10.3389/fimmu.2022.884648.
52. Marin, N.D., Krasnick, B.A., Becker-Hapak, M., Conant, L., Goedegebuure, S.P., Berrien-Elliott, M.M., Robbins, K.J., Foltz, J.A., Foster, M., Wong, P., et al. (2021). Memory-like Differentiation Enhances NK Cell Responses to Melanoma. Clin. Cancer Res. *27*, 4859–4869. https://doi.org/10.1158/1078-0432.Ccr-21-0851.
53. Becker-Hapak, M.K., Shrestha, N., McClain, E., Dee, M.J., Chaturvedi, P., Leclerc, G.M., Marsala, L.I., Foster, M., Schappe, T., Tran, J., et al. (2021). A Fusion Protein Complex that Combines IL-12, IL-15, and IL-18 Signaling to Induce Memory-Like NK Cells for Cancer Immunotherapy. Cancer Immunol. Res. *9*, 1071–1087. https://doi.org/10.1158/2326-6066.Cir-20-1002.
54. Crinier, A., Milpied, P., Escalière, B., Piperoglou, C., Galluso, J., Balsamo, A., Spinelli, L., Cervera-Marzal, I., Ebbo, M., Girard-Madoux, M., et al. (2018). High-Dimensional Single-Cell Analysis Identifies Organ-Specific Signatures and Conserved NK Cell Subsets in Humans and Mice. Immunity *49*, 971–986.e5. https://doi.org/10.1016/j.immuni.2018.09.009.
55. Li, Z.Y., Morman, R.E., Hegermiller, E., Sun, M., Bartom, E.T., Maienschein-Cline, M., Sigvardsson, M., and Kee, B.L. (2021). The transcriptional repressor ID2 supports natural killer cell maturation by controlling TCF1 amplitude. J. Exp. Med. *218*, e20202032. https://doi.org/10.1084/jem.20202032.
56. Zook, E.C., Li, Z.Y., Xu, Y., de Pooter, R.F., Verykokakis, M., Beaulieu, A., Lasorella, A., Maienschein-Cline, M., Sun, J.C., Sigvardsson, M., and Kee, B.L. (2018). Transcription factor ID2 prevents E proteins from enforcing a naïve T lymphocyte gene program during NK cell development. Sci. Immunol. *3*, eaao2139. https://doi.org/10.1126/sciimmunol.aao2139.
57. Liu, J., Wang, Z., Hao, S., Wang, F., Yao, Y., Zhang, Y., Zhao, Y., Guo, W., Yu, G., Ma, X., et al. (2021). Tcf1 Sustains the Expression of Multiple Regulators in Promoting Early Natural Killer Cell Development. Front. Immunol. *12*, 791220. https://doi.org/10.3389/fimmu.2021.791220.
58. Yang, C., Jin, J., Yang, Y., Sun, H., Wu, L., Shen, M., Hong, X., Li, W., Lu, L., Cao, D., et al. (2022). Androgen receptor-mediated CD8(+) T cell stemness programs drive sex differences in antitumor immunity. Immunity *55*, 1268–1283.e9. https://doi.org/10.1016/j.immuni.2022.05.012.

STAR★METHODS

KEY RESOURCES TABLE

REAGENT or RESOURCE	SOURCE	IDENTIFIER
Antibodies		
Anti-mouse-CD45-BUV395	BD Biosciences	Cat#564279; RRID:AB_2651134
Anti-mouse-CD45.2-BV785	BioLegend	Cat#109839; RRID:AB_2562604
Anti-mouse-CD45.1-FITC	eBioscience	Cat#11-0453-82; RRID:AB_469629
Anti-mouse-CD3-APC/Cy7	BD Biosciences	Cat#557596; RRID:AB_396759
Anti-mouse-CD11b-PE/Cy7	BioLegend	Cat#101216; RRID:AB_312799
Anti-mouse-CD27-FITC	eBioscience	Cat#14-0271-82; RRID:AB_467183
Anti-mouse-CD107a-APC	BioLegend	Cat#123137; RRID:AB_2234505
Anti-mouse-MHC class I (H-2kb)-FITC	eBioscience	Cat#11-5958-82; RRID:AB_11149502
Anti-mouse-NK1.1-PercP/Cy5.5	eBioscience	Cat#45-5941-82; RRID:AB_914361
Anti-mouse-CD8a-BV650	BioLegend	Cat#100742; RRID:AB_2563056
Anti-mouse-CD69-PE/Cy7	BioLegend	Cat#104512; RRID:AB_493564
Anti-mouse-CD335(NKp46)-BV510	BioLegend	Cat#137623; RRID:AB_2563290
Anti-mouse-IFN-γ-PE	BioLegend	Cat#505808; RRID:AB_315402
Anti-mouse-IFN-γ-BV711	BioLegend	Cat#505836; RRID:AB_2650928
Anti-mouse-Ki-67-BV605	BioLegend	Cat#652413; RRID:AB_2562664
Anti-mouse-TCF-1-PE	BD Biosciences	Cat#564217; RRID:AB_2687845
Anti-mouse-IFNAR1-PE	BioLegend	Cat#127312; RRID:AB_2248800
Anti-mouse FcR (CD16/CD32)	BioXCell	Cat#BE0307; RRID:AB_2736987
Anti-human FcR	Miltenyi Biotech	Cat#130-059-901; RRID:AB_2892112
Anti-human-CD45-BUV395	BD Biosciences	Cat#563792; RRID:AB_2869519
Anti-human-CD45-PerCP/Cy5.5	BioLegend	Cat#368504; RRID:AB_2566352
Anti-human-CD3-BUV805	BD Biosciences	Cat#612895; RRID:AB_2870183
Anti-human-CD14-PerCP/Cy5.5	BioLegend	Cat#367109; RRID:AB_2566711
Anti-human-CD56-BV650	BD Biosciences	Cat#748098; RRID:AB_2872559
Anti-human-CD16-APC/Cy7	BioLegend	Cat#302018; RRID:AB_314218
Anti-human-CD8-BV421	BioLegend	Cat#344748; RRID:AB_2629584
Anti-human-CD4-BV510	BioLegend	Cat#357419; RRID:AB_2715939
Anti-human-STING-AF647	BD Biosciences	Cat#564836; RRID:AB_2738974
Anti-human-TCF-1-PE	Cell Signaling Technology	Cat#14456; RRID:AB_2798483
Anti-human-IFN-γ-BV650	BD Biosciences	Cat#563416; RRID:AB_2738193
Anti-human-CD107a-PE/cy7	BioLegend	Cat#328617; RRID:AB_11147761
*InVivo*MAb anti-mouse CD8α	BioXCell	Cat#BE0061; RRID:AB_1125541
*InVivo*Plus anti-mouse NK1.1	BioXCell	Cat#BP0036; RRID:AB_1107737
*InVivo*Plus anti-mouse IFNAR1	BioXCell	Cat#BP0241; RRID:AB_2687723
β-Actin (13E5) Rabbit mAb	Cell Signaling Technology	Cat#4970; RRID:AB_2223172
Rabbit Polyclonal anti-Tubulin	Proteintech	Cat#10094-1-AP; RRID:AB_2210695
STING (D2P2F) Rabbit mAb	Cell Signaling Technology	Cat#13647; RRID:AB_2732796
TBK1/NAK Antibody	Cell Signaling Technology	Cat#3013; RRID:AB_2199749
Phospho-TBK1/NAK(Ser172) (D52C2) Rabbit mAb	Cell Signaling Technology	Cat#5483; RRID:AB_10693472
Phospho-STING(Ser366) (E9A9K) Rabbit mAb	Cell Signaling Technology	Cat#50907; RRID:AB_2827656

(*Continued on next page*)

Continued

REAGENT or RESOURCE	SOURCE	IDENTIFIER
Bacterial and virus strains		
DH5α competent cells	Tiangen Biotech	Cat#CB101
Fast-T1 competent cells	Vazyme	Cat#C505
Chemicals, peptides, and recombinant proteins		
Fixable Viability Stain 780	BD Biosciences	Cat#565388; RRID:AB_2869673
Fixable Viability Stain 700	BD Biosciences	Cat#564997; RRID:AB_2869637
2′3′-cGAMP	Invivogen	Cat#tlrl-nacga23; CAS: 1441190-66-4
Collagenase Type I	Worthington Biochemical	Cat#LS004186
Collagenase Type VIII	Sigma	Cat#C2139; CAS: 9001-12-1
DNase I	Sigma	Cat#DN25; CAS: 9003-98-9
DNA transfection reagent	Neofect Biotech	Cat#TF201201
GMPO Polybrene	Genomeditech	Cat#GM-040901B
TRIzol Reagent	Invitrogen	Cat#15596018
Fixation/Perm Diluent	eBioscience	Cat#00-5223-56
Fixation/Permeabilization Concentrate	eBioscience	Cat#00-5123-43
Permeabilization buffer 10X	eBioscience	Cat#00-8333-56
Phosflow Fix Buffer I	BD Biosciences	Cat#557870
Phosflow Perm/Wash Buffer I	BD Biosciences	Cat#557885
Cell stimulation cocktail plus protein transport inhibitor (500×)	eBioscience	Cat#00-4975-93
Protein transport inhibitor	eBioscience	Cat#00-4980-93
Trypan Blue	Gibco	Cat#15250061
Puromycin Dihydrochloride	Beyotime Biotechnology	Cat#ST551
Recombinant Human IL-15	PeproTech	Cat#200-15
Recombinant Human IL-12	PeproTech	Cat#200-12
Recombinant Murine IL-15	PeproTech	Cat#210-15
Recombinant Murine IL-18	MBL	Cat#B002-5
Critical commercial assays		
EasySep™ Mouse NK Cell Isolation Kit	STEMCELL	Cat#19855
E.Z.N.A.® Endo Free Plasmid Midi Kit	Omega Bio-tek	Cat#D6904
BCA Protein Assay Kit	Beyotime Biotechnology	Cat#P0011
DNA ligation kit-Ligation High	TOYOBO	Cat#LGK-100
2 x Taq Master Mix, Dye Plus	Vazyme	Cat#P212
ReverTra Ace qPCR RT Master Mix	TOYOBO	Cat#FSQ-301
SYBR Green Real-time PCR Master Mix	TOYOBO	Cat#QPK-201
Experimental models: Cell lines		
MC38	Lab of Ralph R. Weichselbaum	N/A
B16F10	Cell bank of the Chinese academy of sciences	N/A
MC38-Vector	This paper	N/A
MC38-B2M$^{-/-}$	This paper	N/A
MC38-STING$^{-/-}$	This paper	N/A
MC38-cGAS$^{-/-}$	This paper	N/A
B16F10-Vector	This paper	N/A
B16F10-B2M$^{-/-}$	This paper	N/A
B16F10-STING$^{-/-}$	This paper	N/A
B16F10-cGAS$^{-/-}$	This paper	N/A
MC38-tdTomato	This paper	N/A

(*Continued on next page*)

Continued		
REAGENT or RESOURCE	SOURCE	IDENTIFIER
NK-92MI	Lab of Dr. Hua Zhu	N/A
K562	Lab of Dr. Ying Wang	N/A
HEK293T	Cell bank of the Chinese academy of sciences	N/A
Experimental models: Organisms/strains		
C57BL/6 mice	Shanghai Slaccas	N/A
STING$^{-/-}$ mice	Lab of Glen N. Barber	N/A
cGAS$^{-/-}$ mice	Jackson Laboratory	N/A
Ncr1^{iCre} (C57BL/6-Ncr1tm1(iCre)/Bcgen) transgenic mice	Beijing Biocytogen Co., Ltd	N/A
STING$^{flox/flox}$ mice	Lab of Dr. John C Cambier	N/A
cGAS$^{flox/flox}$ mice	Lab of Dr. Zhenyu Ju	N/A
IFNAR1$^{flox/flox}$ mice	Lab of Dr. Ulrich Kalinke	N/A
CD45.1 congenic mice	Lab of Dr. Chuanxin Huang	N/A
Oligonucleotides		
All oligo sequences used in this paper are listed in Table S1.		Table S1
Recombinant DNA		
lentiCRISPR v2	Lab of Xin-Yuan Liu	N/A
PsPAX2	Lab of Xin-Yuan Liu	N/A
pMD2.G	Lab of Xin-Yuan Liu	N/A
Software and algorithms		
Prism graphpad	GraphPad Prism software	Version 8.0
FlowJo	Tree Star software	Version 10.0
Photoshop	Adobe Systems	Version CS6

RESOURCE AVAILABILITY

Lead contact

Further information and requests for reagents and resources should be directed and will be fulfilled by the lead contact, Liufu Deng (dengliufu@sjtu.edu.cn).

Materials availability

All unique/stable reagents generated in this study are available from the lead contact with a completed materials transfer agreement.

Data and code availability

- All data reported in this paper will be shared by the lead contact upon request.
- This paper does not report original codes.
- Any additional information required to reanalyze the data reported in this work paper is available from the lead contact upon request.

EXPERIMENTAL MODEL AND STUDY PARTICIPANT DETAILS

Mice

Experimental animals were kept under specific pathogen-free (SPF) conditions. Six-to eight-week-old female C57BL/6J (WT) mice were purchased from Shanghai SLAC Laboratory Animal Co., Ltd and all mice were at least doubly housed. STING$^{-/-}$ mice were kindly provided by Dr. Glen N. Barber of University of Miami School of Medicine and backcrossed to C57BL/6J mice for at least ten generations. cGAS$^{-/-}$ mice were purchased from the Jackson Laboratory. CD45.1 mice were gifts from Dr. Chuanxin Huang of Shanghai Institute of Immunology. The Ncr1^{iCre} (C57BL/6-Ncr1$^{tm1(iCre)}$/Bcgen) transgenic mice were obtained from Beijing Biocytogen Co., Ltd. STING$^{flox/flox}$ mice were kindly provided by Dr. John C Cambier of University of Colorado Denver and National Jewish Health. And cGAS$^{flox/flox}$ mice were gifts from of Dr. Zhenyu Ju of the Jinan University. IFNAR1$^{flox/flox}$ mice were kindly provided

from Professor Dr. Ulrich Kalinke of the TWINCORE-Zentrum für Experimentelle und Klinische Infektionsforschung. STING$^{flox/flox}$, cGAS$^{flox/flox}$ and IFNAR1$^{flox/flox}$ mice were crossed with Ncr1^{iCre} mice to generate Ncr1^{iCre}STING$^{f/f}$, Ncr1^{iCre}cGAS$^{f/f}$ and Ncr1^{iCre}IFNAR1$^{f/f}$ mice, respectively. And all *in vivo* animal experiments were carried out in accordance with the animal experimental guidelines set by the Institutional Animal Care and Use Committee (IACUC). This study has been approved by IACUC of Shanghai Jiao Tong University School of Medicine and Shanghai Jiao Tong University.

Cells and cell culture

B16F10 melanoma cells (purchase from national collection of authenticated cell cultures) were maintained in MEM (Hyclone) supplemented with 10% FBS (Gemini), 100 U/mL penicillin (Thermo Fisher Scientific), 100 μg/mL streptomycin (Thermo Fisher Scientific), 1×non-essential amino acids solution (Thermo Fisher Scientific), 1 mM sodium pyruvate (Thermo Fisher Scientific) and 10 mM HEPES (Thermo Fisher Scientific) at 37°C in 5% CO_2. MC38 colon tumor cells (gifted from Dr. Yang-Xin Fu) and K562 tumor (kindly provided by Dr. Ying Wang), were cultured in DMEM (CORNIG) supplemented with 10% FBS, 100 U/mL penicillin, 100 μg/mL streptomycin and 10 mM HEPES at 37°C in 5% CO_2. B2M$^{-/-}$ and cGAS$^{-/-}$ cell lines were generated using CRISPR-Cas9 (described below). Primary NK cells obtained from mouse and human PBMC were cultured in cultured in RPMI 1640 (GIBCO) supplemented with 10% FBS (GIBCO), 100 U/mL penicillin, and 100 μg/mL streptomycin, 4 mM L-glutamine, 50 μM 2-Mercaptoerhanol, 1 mM sodium pyruvate. The NK-92MI cell line (kindly gifted by Dr. Hua Zhu) were cultured in α-MEM medium (Gibco) containing 12.5% horse serum (Hyclone), 12.5% fetal bovine serum (Gibco), 0.02 mM folic acid (Sigma), 0.2 mM inositol (Sigma), 1% penicillin/streptomycin, 0.1mM β-mercaptoethanol. All the cells were tested negative for mycoplasma contamination.

Human samples collection

All the primary, metastatic and adjacent carcinoma specimens were obtained under informed consent from untreated patients undergoing surgical resection. Human peripheral blood samples were obtained from healthy volunteers and patients with cancer (cervical, endometrial and ovarian cancer) (Table S2). The healthy control samples were obtained from individuals with no known cancer or other diseases. The study was performed in accordance with the protocols approved by the institutional review board of Ren Ji Hospital, Shanghai Jiao Tong University School of Medicine and informed consent from all subjects has been obtained. Peripheral blood was collected for the further isolation of peripheral blood mononuclear cells (PBMCs) as previously described.[58] Briefly, blood was diluted with an equal volume of PBS, overlaid on Ficoll-Paque PLUS (GE Healthcare) and centrifuged at 2000 rpm for 20 min at 20°C. Mononuclear cells were washed twice with PBS and either used immediately or frozen in fetal bovine serum containing 10% dimethyl sulfoxide stored at −80°C until use.

METHOD DETAILS

Generation of cell lines using CRISPR-Cas9

The genome editing one vector system (lentiCRISPR-v2) (from the laboratory of X.-Y. Liu) was used to knockout mouse B2M or cGAS in MC38 and B16F10 tumor cells. The single-guide RNA (sgRNA) oligos targeting murine *Cgas* and murine *B2m* were annealed to generate sgRNA oligonucleotides and then cloned into lentiCRIPR-v2 vector plasmid, respectively. The sequence of the sgRNA were showed in the Table S1. For cGAS knockout, lentiviral particles were generated by co-transfection of HEK293T with lentiCRISPR (with *Cgas* sgRNA cloned) and packaging plasmids PsPAX2 and pMD2.G using NEOFECT DNA transfection reagent (Neofect (beijing) biotech). Supernatants from HEK293T were collected 48 h and 72 h post-transfection, passed through a 0.45 μm filter to remove cell debris and frozen as 1-mL aliquots at −80°C. MC38 and B16F10 were infected with lentivirus in the presence of 10 μg/mL polybrene. 3 μg/mL puromycin (Beyotime Biotechnology) was used to select CRISPR-Cas9-infected MC38 tumor cells and 2 μg/mL puromycin for selection of transduced B16F10 tumor cells. Then these selected knockout clones were confirmed by immunoblot analysis for the loss of cGAS proteins. Two independent clones were analyzed as indicated and the MC38-vector cells were used as control.

For B2M knockout, we transfected tumor cells with lentiCRISPR (with *B2m* sgRNA cloned) plasmid to transiently express the CRISPR-Cas9 system. Transfection was carried out using Lipofectamine 3000 (Invitrogen) and Opti-MEM (Gibco), according to the manufacturer's instructions. After 48 h, cells were cultured with puromycin for four days and the presence of B2M was verified by flow cytometry analysis. Briefly, transfected tumor cells were incubated with 20 ng/mL IFN-γ (PeproTech) for 48 h to induce MHC class I expression and followed identified B2M knockout cell clones via staining with anti-MHC class I (H-2Kb; clone AF6-88.5, BioLegend).

In vivo tumor models

For the subcutaneous tumor mouse model, tumor cells were washed three times by PBS and 100 μL cell suspensions were injected subcutaneously. Tumor size was measured using a manual caliper and estimated using the ellipsoid formula: V = L*W*H/2. Tumors were excised before exceeding the volume permitted by the IACUC guidelines for the Shanghai Jiao Tong University. For the metastasis, 200 μL B16F10 melanoma cell suspensions (containing 2×10^5 cells) were intravenously injected into the tail vein of mice. After 12–14 days, the lungs were resected after perfusion with PBS. Lung colonization was quantified by counting the visible colonies on the lung surface under a stereo microscope. For CD8$^+$ T cell depletion, 250 μg anti-CD8 antibody (clone 2.43, BioXCell) was injected

i.p. into the mice every 3 days for total 3 times beginning on day 4 after intravenous tumor inoculation. For NK cell depletion, 250 μg anti-NK antibody (clone PK136, BioXCell) was injected i.p. into the mice every 3 days for total 3 times beginning on day 4 after intravenous tumor inoculation.

Antibodies and flow cytometry

Fluorochrome-conjugated antibodies against mouse proteins were used for flow cytometry: anti-CD45.2 (clone 104, BioLegend), anti-CD45.1 (clone A20, eBioscience), anti-CD3 (clone 145-2C11, BD), anti-NK1.1 (clone PK136, eBioscience), anti-CD69 (clone H1.2F3, BioLegend), anti-NKp46 (clone 29A1.4, BioLegend), anti-CD27 (clone LG.7F9, eBioscience), anti-CD11b (clone M1/70, BioLegend), anti-MHC class I (clone AF6-88.5, BioLegend), anti-IFNAR1 (clone MAR1-5A3, BioLegend), anti-IFN-γ (clone XMG1.2, BioLegend), anti-CD107a (clone 1D4B, BioLegend), anti-TCF-1 (clone S94 -966, BD), anti-Ki-67 (clone 16A8, BioLegend). And antibodies against to human specific markers were as follows: anti-CD45 (clone 2D1, Biolegend), anti-CD3 (clone SK7, Biolegend), anti-CD14 (clone 63D3, BioLegend), anti-CD56 (clone NCAM16.2, BD), anti-CD16 (clone 3G8, BioLegend), anti-IFN-γ (clone 4S.B3, BD), anti-CD107a (clone H4A3, Biolegend), anti-TCF-1/TCF-7 (PE conjugated) (clone C63D9, Cell Signaling Technology), anti-STING (clone T3-680, BD). Flow cytometry was performed using standard protocols as previously described.

Dissected tumor tissues were cut into small pieces and digested with 1 mg/mL collagenase I (Worthington Biochemical) and 0.2 mg/mL DNase I (Sigma) for 30 min at 37°C. Lungs were cut into small pieces and digested by 0.4 mg/mL collagenase VIII (Sigma) and 0.1 mg/mL DNase I (Sigma) for 45 min at 37°C. Single-cell suspensions of all the tissues were generated by passing cells through a 40-μm filter and then blocked with murine anti-FcR (2.4G2, BioXcell) or human anti-FcR (Miltenyi Biotec) for 15 min prior to staining with antibodies against surface molecules at 4°C for 30 min. LIVE/DEAD stain (ThermoFisher Scientific) was used to exclude dead cells. For intracellular staining of transcription factors and cytokines, cells were fixed with the Foxp3/Transcription Factor Staining Buffer Set (eBioscience) according to the standard protocols. For analysis of NK cell function, cell suspensions were incubated for 4 h in medium containing eBioscience Cell Stimulation Cocktail (plus protein transport inhibitors) (Invitrogen), and anti-CD107a (1 μg/mL) antibodies before surface and intracellular staining.

For quantifying the phosphorylation of STING in NK cells from patients with cancer, PMBCs were stimulated with 5 μM cGAMP for 4 h and then harvested to further fixed with Phosflow Fix Buffer I (BD) according to BD Phosflow protocol. The first antibody-Rabbit anti-human p-STING (Ser366) (clone E9A9K, Cell Signaling Technology) was used at a dilution of 1:200. After 30-min incubation, Goat anti-rabbit IgG Alexa Flour 488 (Thermo Fisher Scientific) as the secondary antibody was added at a dilution of 1:2000 for another 30-min incubation and then washed twice with Phosflow Perm/Wash buffer I (BD) for further flow analysis. Flow cytometry was performed using an LSRFortessa or an LSRFortessa X-20 (BD Biosciences). Data were analyzed with FlowJo X.

For quantifying the phosphorylation of TBK1 in NK cells from tumor-bearing mice, 1×10^6 B16F10-vector and B16F10-cGAS$^{-/-}$ cells were injected (intraperitoneally) into WT mice and after 16 h, mouse peritoneal lavage fluid was stained for *p*-TBK1 expression according to BD Phosflow protocol. The first antibody-Rabbit anti-mouse *p*-TBK1 (Ser172) (clone D52C2, Cell Signaling Technology) was used at a dilution of 1:200. And Goat anti-rabbit IgG Alexa Flour 488 (Thermo Fisher Scientific) as the secondary antibody was added at a dilution of 1:2000. Flow cytometry was performed using an LSRFortessa or an LSRFortessa X-20 (BD Biosciences). Data were analyzed with FlowJo X.

Mouse NK cell enrichment and *in vitro* analysis

Enrichment of mouse NK cells from spleens was performed by flow sorting (typically 97% purity). To characterize NK cells activity under STING signaling activated, purified NK cells were seeded in the 96-well plates and stimulated with indicated concentration of cGAMP in the presence of murine IL-15 (10 ng/mL, Peprotech) for 24 h and then quantified expression of CD69 by flow cytometry. For IFNAR1 blockade experiment, 200 μg/mL α-IFNAR1 blocking monoclonal antibody (clone MAR1-5A3; Bio X Cell) was added in the NK cells culture medium along with the exposure to 5 μM cGAMP. For evaluation of the activation of type I interferon signaling, primary NK cells were incubated for 9 h with or without 5 μM cGAMP and then collected for further examination by real-time PCR.

Human NK cell enrichment and *in vitro* analysis

Enrichment of human NK cells from PBMCs obtained from healthy volunteers was performed using the EasySep Human NK Cell Isolation Kit (catalog no. 17955, STEMCELL Technologies) in accordance with the manufacturer's instructions. Isolated human NK cells were pre-activated in the presence of recombinant human IL-15 (5 ng/mL, Peprotech) for 16 h in the 96-well plate and then incubated with or without 1 μM cGAMP in the culture medium for 7 days. After that, these activated cells were collected for further flow analysis. For function evaluation, these cells were re-stimulated by co-culturing with K562 targets (effector/target ratio of 5:1), Protein transport inhibitor (Cat#00-4980-93, Invitrogen) and anti-human CD107a was added after 1 h. The effector and target cells were mixed and centrifuged at 50g for 0.5 min and were incubated at 37°C in 5% CO_2 for 6 h. And then cells were stained with surface markers and intracellular anti-human IFN gamma.

Mouse NK cells co-transfer

In the WT and STING$^{-/-}$ NK cells co-transfer experiment, WT (CD45.1$^+$) and the STING$^{-/-}$ (CD45.2$^+$) donors were on the B6 background. In brief, the spleen cell suspension obtained from CD45.1$^+$ WT and CD45.2$^+$ STING$^{-/-}$ mice were both labeled with CTV (3 μM) and subsequently primary NK cells were enriched for further stimulated with a cytokine cocktail containing IL-12

(10 ng/mL, Peprotech), IL-15 (10 ng/mL, Peprotech) and IL-18 (50 ng/mL, MBL) for 16 h. After that, a 50:50 mixture of CTV-labeled WT and STING$^{-/-}$ NK cells (~5×10^5 cells in total) were intravenously transferred into CD45.1$^+$ CD45.2$^+$ recipient mice. Additionally, these recipients were inoculated with 8×10^5 tumor cells via tail vein 1 h before NK cell injection. Four days or seven days later, transferred-NK cells were characterized through harvesting spleens and lungs by using flow cytometry.

Quantitative reverse transcription PCR

Total RNA was extracted using the TRIzol Reagent (Thermo Fisher Scientific). Reverse transcription of mRNA was performed with ReverTra Ace qPCR RT Master Mix (Toyobo) following the standard protocol. qPCR was performed in SYBR Green Real-time PCR Master Mix (Toyobo) in 7500 Fast Real-Time PCR System or ViiA 7 Real-Time PCR System with 384-Well Block (Applied Biosystems). Data were normalized to the transcription of ACTB. Primers used in this study were included in Table S1.

Detection of DNA in cytosolic extracts

2-3×10^6 MC38-tdTomato cells were intravenously injected into the tail vein of mice. The MC38-tdTomato cells were sorted from the lungs by flow cytometry three days after inoculation. The cytosolic DNA inside the tumor cells were detected as previously described.[13] Briefly, the isolated tumor cells were divided into two equal aliquots. One aliquot was lysed in 50 μM NaOH, boiled for 15 min and then neutralized with 1 M Tris-HCl pH 8 to get normalization controls for total DNA. The other aliquot was lysed for collecting cytosolic supernantants with cytosolic extract buffer (containing 150 mM NaCl, 50 mM HEPES and 25 μg/mL digitonin (Sigma)) following plasma membrane permeabilization. DNA from whole cell lysates or cytosolic extract was obtained with DNA Clean & Concentrator (ZYMO RESEARCH) and assessed by q-PCR with gDNA primers and mtDNA primers. Primers used in this study were included in Table S1.

mtDNA depletion

B16F10 melanoma cells were developed in the presence or absence of 50 μM dideoxycytidine (ddC; Sigma-Aldrich). The mtDNA abundance was assessed by q-PCR analysis at indicated time points. After treatment with ddC for 6 days, tumor cells were harvested and injected to mice via tail vein for further monitoring the generation of lung metastatic tumor nodules.

Western blotting

For exanimating STING knockout efficiency in conditional knockouts, primary NK cells were enriched from spleen of STING$^{flox/flox}$ and Ncr1^{iCre}STING$^{flox/flox}$mice using the EasySep Mouse NK Cell Isolation Kit and lysed in cell lysis buffer for western blotting. For detecting STING pathway activation *in vitro*, NK-92MI cell lines were cultured with or without cGAMP (5 μM) for 6 h and harvested for further analysis of phosphorylation of STING and TBK1. The samples were loaded on SDS–polyacrylamide gel electrophoresis (SDS-PAGE) gels, electrophoresed, transferred onto polyvinylidene difluoride (PVDF) membranes (Millipore), and further incubated with the primary and secondary antibodies. After three more washes in TBS-Tween, blots were reported using the SuperSignal West Pico Chemiluminescent Substrate (Thermo Fisher Scientific). The following primary antibodies were obtained from Cell Signaling Technology: anti-STING (D2P2F) (catalog no. 13647), anti–Phospho-STING (Ser366) (D7C3S) Rabbit mAb (catalog no. 19781), rabbit anti-TBK1 (catalog no. 3013), anti–phospho-TBK1(S172) (D52C2) (catalog no. 5483); and from Proteintech: anti-tubulin (catalog no. 10094-1-AP) and anti-β-actin (catalog no. 20536-1-AP).

QUANTIFICATION AND STATISTICAL ANALYSIS

Statistics were performed using Prism8 (GraphPad). Unpaired two-tailed Student's t tests or one-way analysis of variance (ANOVA) with Bonferroni's multiple comparison tests were used when data fit the normal distribution. In some instances, paired Student's t tests were used. Data that were not normally distributed were calculated by Wilcoxon matched-pairs signed rank tests (two paired groups) or Kruskal-Wallis test (>2 groups) with Dunn's multiple comparisons. For tumor growth, two-way analysis of variance (ANOVA) was used. For survival curve, statistics were calculated using the log rank (Mantel-Cox) test. The number of biological or technical replicates for each experiment is indicated in the figure legends and all data were presented as mean ± standard error of the mean (SEM). Significance is indicated as follows: *$p < 0.05$; **$p < 0.01$; ***$p < 0.001$; ****$p < 0.0001$; ns, no significant difference.